2018 Early Career Scientist Forum

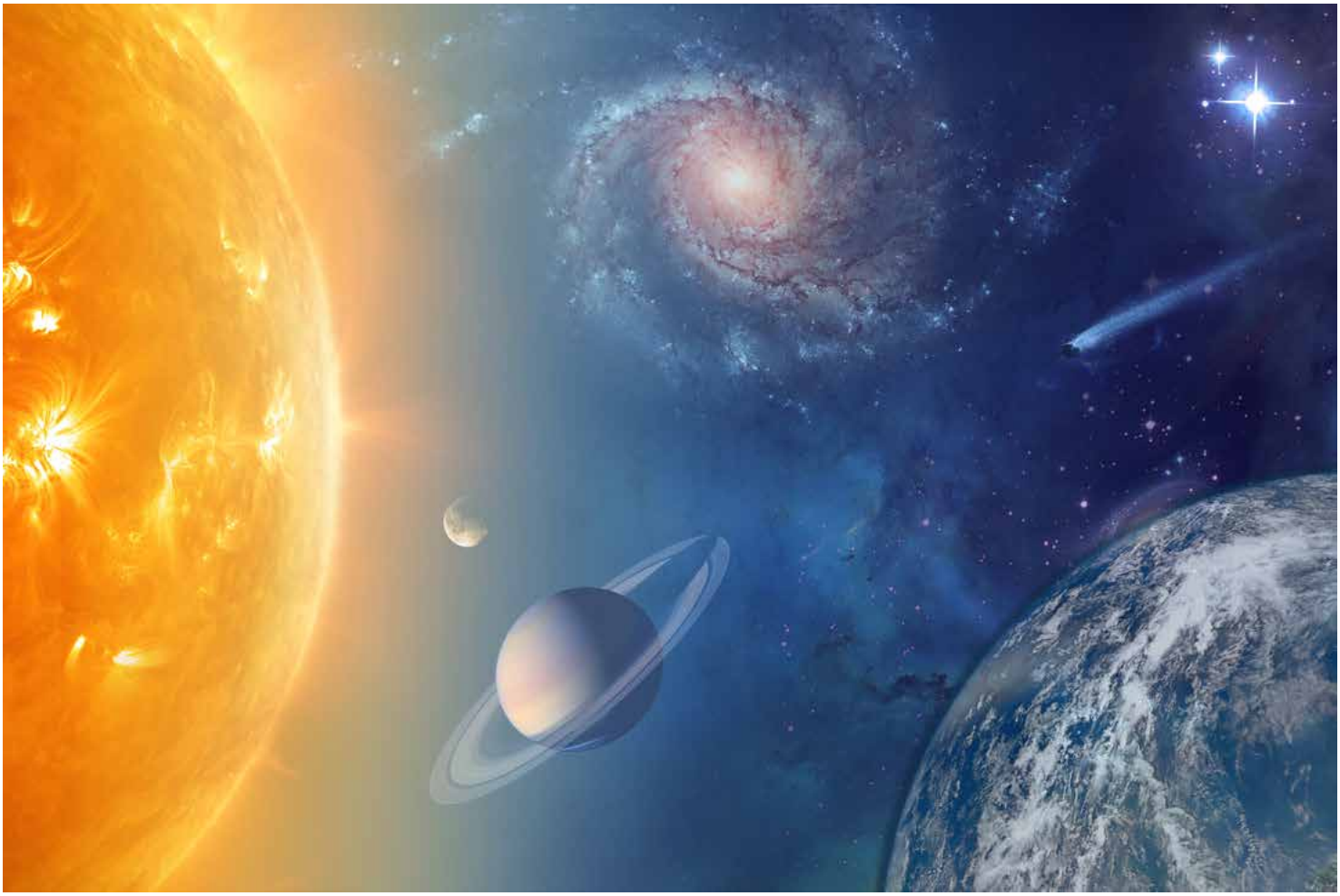

November 1, 2018

GSFC B34 W120-W150

organized by the *Science Director's Committee*

Forum Organizers: Erwan Mazarico (698), Lauren Andrews (610.1), Manuela Girotto (610.1), Stephen Munchak (612), Manisha Ganeshan (613), Edward Nowottnick (614),Gregory Mosby (665), Knicole Colon (667), James Leake (671), Erin Dawkins (674), Giada Arney (693)

Program Overview

The Early Career Scientist Forum (previously the Young Scientist Forum) is a 1-day AGU style conference for our scientists who have obtained their degree in the last 10 years. Any contractor, civil servant, postdoc, university-affiliated scientist, visiting scientist, or graduate student from the Sciences and Exploration Directorate (Code 600) can present, and everyone is invited to attend.

The idea is to provide a chance for early career scientists to showcase their work, get feedback from other scientists, get to know their peers, and to promote future collaboration.

We hope you enjoy the sessions from all four SED Divisions!

Time		**W150**	**W120A**	**W120B**
9:00am	9:15am	**Opening Remarks** Mark Clampin	N/A	N/A
9:15am	10:30am	Session 1A **Data & Tools** (p. 1)	Session 1B **Clouds & Aerosols** (p. 4)	Session 1C **Comets & Mars** (p. 8)
10:30am	10:45am	Break		
10:45am	12:00pm	Session 2A **Planetary Geophysics** (p. 12)	Session 2B **Galaxies & Cosmology** (p. 16)	Session 2C **Air Quality** (p. 19)
12:00pm	12:45pm	Lunch / Poster setup		
12:45pm	2:00pm	Session 3A **Earth & Analogs** (p. 23)	Session 3B **Ocean & Ice** (p. 27)	Session 3C **Jupiter & Titan** (p. 31)
2:00pm	2:15pm	Break		
2:15pm	3:30pm	Session 4A **Heliophysics** (p. 34)	Session 4B **The Water Cycle** (p. 37)	Session 4C **Exoplanets** (p. 40)
3:30pm	5:00pm	**Poster Session** (p. 43)		

An author index can be found on page 71.

Session 1A: Data and Tools

Session chairs: Lauren Andrews & Manuela Girotto

Ushering in a New Frontier in the Earth and Space Sciences Through Data Science

1A-01
9:15am
W150

Ryan McGranaghan (675)

Brian Wilson (NASA JPL), Anthony Mannucci (NASA JPL), Chris Mattmann (NASA JPL)

The hallmarks of the geospace system, which extends from the near Earth space environment, through the magnetosphere and interplanetary space, to the Sun, are variability and complexity. To unravel the critical variabilities and complexities and to evolve beyond current approaches to understand geospace, new data-driven approaches and data analysis technologies are required. These data-driven methods are taking on new importance in light of the shifting data landscape of the geospace system. The space physics community faces both an exciting opportunity and an important imperative to create a new frontier built at the intersection of traditional approaches and state-of-the-art data-driven sciences and technologies. This talk will first discuss the meaning of data science in the context of geospace, and then reveal efforts from a Jet Propulsion Laboratory Data Science Working Group pilot project to leverage data science innovation to utilize a powerful data set for geospace science – Global Navigation Satellite Systems (GNSS) signals. We take advantage of a large volume of GNSS data, increasingly sophisticated tools for data-driven discovery, and machine learning algorithms covering a spectrum of complexity to develop novel predictive models of space weather-driven disruptions to GNSS signals (i.e., scintillation). We find that machine learning approaches significantly outperform current predictive capabilities, which, at high-latitudes, only consist of climatology and persistence. Using a robust metric known as the Total Skill Score (TSS), we position our results as a benchmark upon which to evaluate future predictive models, following a similar approach developed by the solar flare prediction community [Barnes et al., 2016]. Finally, this talk will be targeted to spark discussion of how data science provides a common paradigm to bridge disciplines (particularly across the Earth and Space Sciences), leading to the opening of new interdisciplinary research vistas and future funding opportunities for geospace science.

G. Barnes et al., (2016), A comparison of flare forecasting methods. I. Results from the "All Clear" workshop, The Astrophysical Journal, 829(2), 89.

1A-02
9:30am
W150

Capacity Building with NASA's Applied Remote Sensing Training Program

Elizabeth Hook (613)

Ana Prados (614), Brock Blevins (614)

NASA's Applied Remote Sensing Training program (ARSET), seeks to empower the global community to make better decisions through remote sensing trainings. By providing in-person and online trainings, ARSET has provided more than 100 trainings and had more than 13,000 participants since it began in 2008. In developing and providing trainings, ARSET serves as a bridge between decision-makers, Earth observations, and tool developers. As a result of nine years of training, attendee data, and feedback from decision-makers, ARSET can provide insight into the professions of training attendees, how useful they find Earth observing tools for professional applications, and what the program has learned from its monitoring and evaluation practices.

1A-03
9:45am
W150

The MARA System and Its Applications

Galina Wind (613)

Kerry Meyer (613), Steven Platnick (610.8)

The heritage operational methodology for generating gridded statistical aggregations of Atmosphere Product retrievals (e.g., cloud, aerosol, atmospheric water vapor, etc.) from the MODerate resolution Imaging Spectroradiometer (MODIS) is generally quite static. Adding or modifying statistical capabilities is a time and labor-intensive task. The current algorithm and aggregated products (MOD08/MYD08 for Terra/Aqua MODIS, respectively) are also tightly coupled to the MODIS instrument and only support serial execution. Because of these limitations, it has not been possible to utilize the existing aggregation algorithm for research-level global analyses of the MODIS products. For example, variable or geographic data sub-setting and/or aggregation resolution changes have not been an option. The existing algorithm has also suffered from various portability issues due to its dependence on custom toolkits.

The research-level Multi-instrument Atmospheric Retrieval Aggregation (MARA) system has been developed to address these challenges. MARA is a flexible, modular, cross-platform code written in a mix of Fortran90 and C without any custom toolkits. It uses a fully external instrument, aggregation type, variable and statistic specification, and fully automates output variable name and type generation removing the heavy labor component of the MOD08/MYD08 file specification process. The MARA system also externalizes specification of aggregation resolution and any temporal constraints, and features customizable geographical sampling options via, e.g., pre-defined regular boxes or irregular coordinate sets such as the shape of a section of a country. Furthermore, the MARA system supports multiple parallelization levels determined by the problem size in order to optimize computing resource use.

In this presentation we will show the current implementation of the MARA system and show analyses that previously would have been prohibitively expensive to perform.

Forecast Sensitivity and Observation Impact (FSOI) Inter-comparison Experiment

1A-04
10:00am
W150

Rahul Mahajan (610.1)
Dan Holdaway (610.1), Ron Gelaro (610.1)

Forecast Sensitivity and Observation Impact (FSOI) techniques provide a practical means to estimate the forecast impact of all assimilated observations for NWP systems. In this presentation, we describe direct comparisons of FSOI quantities between different NWP systems. A common "baseline" set of FSOI experimental parameters are applied for the time period December-February (DJF) 2014/2015. An adjoint-based FSOI approach (Langland and Baker, 2004) is applied for the NWP systems at NASA/GMAO, the Naval Research Laboratory (NRL), the UK Met Office (UKMet); where as an ensemble-based FSOI approach (Kalnay et al., 2012) is applied at the National Centers for Environmental Prediction (NCEP). The Japan Meteorological Agency (JMA) applies both the adjoint-based and ensemble-based FSOI capabilities, enabling a direct comparison between the two techniques. Given the aforementioned experiment, we plan to describe the differences in aggregated FSOI quantities between NWP systems for the relevant observing systems. Additionally, NWP system inter-comparisons of FSOI quantities for common observation subsets within the 3-month period will be presented. The comparisons of observation subsets will provide insight as to the extent to which the aggregate results are representative in both space and time. This is an extension to the previous work done by Gelaro et al. (2010) on the THORPEX Observation Intercomparison Experiment.

SAPHIRA: A New NIR APD Array

1A-05
10:15am
W150

Dani Atkinson (665)

Introduced by the Leonardo Corporation, the SAPHIRA is a new detector that uniquely is capable of NIR photon-counting across an array. With a fast readout and low dark current the device has quickly become the backbone of NIR adaptive optics and is being deployed on several terrestrial telescopes. I believe it opens new applications for future space telescopes, including exoplanetary studies.

Session 1B: Clouds and Aerosols

Session chairs: Ed Nowottnick & James Leake

Fractionation of δ13C in Titan's Atmosphere through Aerosol Formation

1B-01
9:15am
W120A

Scott Tewksbury Wieman (699)

Melissa S. Ugelow (691), Melissa G. Trainer (699), Jennifer C. Stern (699), Madeline C. Roach (University of Northern Iowa)

Titan, with its thick atmosphere, lakes of liquid hydrocarbons, and subsurface water ice, is an important system to study for our understanding of prebiotic chemistry. While the Cassini-Huygens mission measured the isotopic fractionation (δH, δ13C, δ5N, δ8O) of several major gas-phase atmospheric components, it never conclusively measured isotopic fractionation of airborne aerosols. Laboratory studies have since measured the carbon isotopic fractionation of Titan photochemical aerosol analogs and found that they are enriched compared to the initial gas from which they form. Our work focuses on the inverse of this, studying the changes that occur in the surrounding gas-phase species as Titan-like aerosols are formed in a recirculating chamber. We monitored the δ13C fractionation and abundance of the major carbon-bearing gas-phase species (methane, ethane) and the abundance of additional trace gas species on an hourly basis during single- and multi-day experiments. We observe that the gas mixture also becomes enriched over the course of aerosol formation, which is counter to our expectations of atmospheric depletion due to the formation of enriched aerosols. We also report the volumetric fractionation present in our system as a possible background present in our data. Further work is aimed at isolating, concentrating, and measuring the fractionation of trace gas species such as propane in order to better understand reaction pathways, fractionation pathways, and the light isotope sink.

Ongoing neural network algorithm development for polarimetric observations of clouds and aerosols above clouds

1B-02
9:30am
W120A

Daniel Miller (616)

Kirk Knobelspiesse (616), Michal Segal-Rozenheimer

We have developed a multi-layer neural network (NN) based algorithm for the retrieval of cloud microphysical properties (cloud optical depth, cloud droplet effective radius and variance) from airborne multi-angle polarimetric measurements. This feed forward back-propagation multi-layer perceptron network is developed and applied to data from the airborne Research Scanning Polarimeter (RSP) instrument. RSP measures both polarized and total reflectance in the spectral range of 410 to 2260 nm and scans along the flight track obtaining ∼150 viewing zenith angles spanning -60° to 60". The neural network architecture training, and input parameters were developed using a synthetic training set and informed

by an information content analysis (Segal-Rozenhaimer, 2018 in process). In this study, we present further development of the algorithm, including the correction for output parameters based on comparisons to existing retrieval algorithms using data from the ObseRvations of Aerosols above CLouds and their intEractionS (ORACLES) 2016 and 2017 NASA field campaign. We will also discuss our approach toward extending the lessons from this NN exercise to retrievals of more complicated remote sensing systems - such as simultaneous retrieval of aerosol and cloud properties

---

The Relationship Between Cirrus Properties and Dynamic Formation Mechanism Using Airborne and Space-Based Lidars

1B-03
9:45am
W120A

John Yorks (612)

Matt McGill, Scott Ozog, Bastiaan van Diendenhoven, Brian Cairns, Sarah Woods

Cirrus clouds have a significant effect on the Earth's radiation budget and climate due to their prevalence in the tropics and mid-latitudes. Quantifying these effects remains a challenge due to a lack of studies across the wide spectrum of cirrus properties and dynamic formation mechanisms, uncertainties in cirrus model parameterizations, and the difficulties of measuring cirrus in situ. In this study, we examine the relationship between thin cirrus cloud properties and dynamic formation mechanism using airborne and space-based lidar. Specifically, we will compute statistics of thin cirrus properties from the Cloud Physics Lidar (CPL), which has flown more than 100 flights on NASA high-altitude aircraft. Case studies are explored using coincident measurements of cirrus microphysical properties from polarimeters and in situ cloud probes. Cloud-Aerosol Transport System (CATS) lidar measurements from the Intentional Space Station (ISS) provide global perspective of cirrus properties that complement the CPL dataset. The lidar ratios and depolarization ratios retrieved from CPL and CATS for thin cirrus clouds formed by synoptic-scale uplift over land are lower than convectively-generated thin cirrus over tropical oceans. These higher depolarization ratios for tropical thin cirrus are likely a consequence of colder cloud temperatures and the presence of more column-shaped ice particles (observed by the in situ probes) compared to mid-latitude thin cirrus. CPL thin cirrus backscatter color ratios are directly proportional to depolarization ratio for synoptically-generated cirrus, suggesting particle shape is a function of particle size. Given that uncertainties in particle shape parameterizations can produce errors in the cirrus radiative forcing estimates greater than 60 percent, the relationship between cirrus properties and dynamic formation mechanism needs to be considered when studying the impact of cirrus on the Earth's climate system.

1B-04
10:00am
W120A

Comparing Lidar and In-Situ Retrieved Cirrus Properties and Associated Differences in TOA Cloud Radiative Forcing

Scott Ozog (612)
Matt McGill (612), John Yorks (612)

Cirrus are the most common cloud type in our atmosphere (Stubenrauch et al. 2013), and play a crucial role in modulating Earth's radiative energy balance. Due to their complexity, cirrus are poorly represented in global circulation models (GCM), and are a significant source of their uncertainty. They are the only cloud type that can have a positive net daytime cloud radiative forcing (CRF) at the top of the atmosphere (TOA), however, depending on their microphysical properties can also have a net cooling affect (Zhang et al. 1999). Lidar instruments provide valuable vertical profiles of cirrus layer extinction, ice water content (IWC), and particle size; which are incorporated into radiative transfer models (RTM). The NASA Cloud Physics Lidar (CPL) has flown on multiple campaigns in collaboration with in-situ probes aimed at measuring these same variables. It is paramount in understanding remote sensing products how they compare to their in-situ counterparts, and furthermore what these differences mean for models incorporating these variables as input. The SEAC4RS, ATTREX, and REThinC field campaigns were conducted in 2013, 2014, and 2017, respectively. The SPEC Inc. in-situ probes flew on conjunction with CPL in all campaigns providing coincident retrievals of cirrus microphysical and optical properties. Here, profiles of cirrus properties will be compared between the CPL remote sensing retrievals, and those from the in-situ probes. The libRadtran (library of radiative transfer, Mayer and Kaylling, 2005) RTM will be tasked with performing radiative transfer simulations to contrast the difference in estimated TOA CRF. These comparisons provide valuable insight into the potential errors induced into CRF estimates along with the impact and importance of correctly parameterizing cirrus microphysical and optical properties.

1B-05
10:15am
W120A

Using laboratory methods under extreme conditions to better understand refractory cloud formation in exoplanet atmospheres

Erika Kohler (691)
Frank Ferguson (691)

The high number of extrasolar planets found in recent years has challenged our knowledge of solar system sciences. These recently discovered planets show a large diversity in their masses, temperatures, orbital periods, and other properties. With such a diverse mix of planetary parameters, it is safe to assume that the atmospheric properties are just as varied. Evidence suggests the presence of silicate and metal condensates in their atmospheres. This has led to new insights into the physics of cloud formation, and new observational data will help test and validate theoretical models. However, these models are fundamentally limited by the insufficiencies of laboratory data on the properties of atmospheric constituents; new laboratory data is desperately needed to advance state-of-the-art of exoplanet atmospheric models. A laboratory verification of the condensation and vaporization predictions of refractory materials is critically needed in order to inform and improve atmospheric and spectral

models. The stability of forsterite (Mg_2SiO_4) and iron (Fe) were tested in a thermogravimetric balance at NASA Goddard Space Flight Center. The minerals were pumped under vacuum for twenty-four hours at room temperature and then heated to a predetermined high temperature, dependent on the expected vaporization temperature of that material. After observing mass loss, the temperature is lowered at preset durations and mass measurements are taken in similar measured increments. The data is processed by a computer program in order to calculate the mass loss as a function of temperature. The direct output of these experiments is the actual measured vapor pressures of minerals at high temperatures, which are used to predict the temperature regimes for stable cloud formation. These temperature regimes are then used as inputs to atmospheric models that predict cloud condensates. Presently, inputs for models of exoplanet atmospheres depend heavily upon extrapolations from terrestrial pressures and atmospheres. This work will lead to significant improvements in the accuracy of exoplanet atmospheric models by eliminating the need to extrapolate data from terrestrial conditions.

Session 1C: Mars and Comets

Session chairs: Erwan Mazarico & Knicole Colon

The Volatile Composition of CO-Dominated Comet C/2016 R2 (PANSTARRS)

1C-01
9:15am
W120B

Adam McKay (693)
Michael DiSanti (693)

In December 2017 we obtained spectra of comet C/2016 R2 (PanSTARRS) that were extremely atypical for comets observed at optical wavelengths. Usually dominated by neutral species such as CN and C2, the optical spectrum of C/2016 R2 was devoid of these features and was instead dominated by ionic emissions from CO+ and N_2+, with the N_2+ detection being the most secure detection of N_2+ in a comet obtained in the age of digital detectors (Cochran and McKay 2018). Sub-mm observations showed strong CO emission (Wierzchos and Womack 2018, de Val Borro et al. 2018, N. Biver accepted), confirming the hypervolatile-rich nature of this comet suggested by the optical spectra. We present additional observations of comet C/2016 R2 (PanSTARRS) obtained with the IRAC instrument on the Spitzer Space Telescope, iSHELL on the NASA IRTF, ARCES at Apache Point Observatory (APO), and the Tull Coude Spectrograph and the Prime Focus Corrector (PFC) at McDonald Observatory aimed at characterizing the volatile composition of this unusual comet. We report detections of four species (CO, CH_4, CO_2, and N_2+) and provide sensitive upper limits on six other species (C_2H_6, CH_3OH, H_2CO, CN, NH_2, and OH). CN is employed as a proxy for HCN, NH2 for NH3, N_2+ for N_2, and OH for H_2O. For all detected species, we measure strong enhancements relative to our derived H_2O upper limit by one to two orders of magnitude compared to other comets observed to date. All species are heavily depleted relative to CO compared to other comets, except N_2, which is enhanced. Unlike all other comets for which constraints on HCN, NH_3, and N_2 are available, N_2 seems to be the dominant nitrogen-bearing volatile in C/2016 R2. We will discuss our measured abundances of key species and discuss implications for the chemistry in the early Solar System. This work makes use of Director's Discretionary Time observations obtained on Spitzer, IRTF, and APO, and we thank these observatories for granting our group DDT time to conduct these observations. This work is funded through the NASA NPP program, administered by USRA.

Quantifying the Evolution of Molecular Composition of comet 21P/Giacobini-Zinner

1C-02
9:30am
W120B

Sara Faggi (690)

Michael Mumma (690), Geronimo Villanueva (693), Lucas Paganini (693)

21P/Giacobini-Zinner has been described as one of the brighter comets of Jupiter's dynamical family. Optical observations of free radicals showed that 21P/G-Z was severely depleted in C2 relative to CN, leading to a dichotomy in the carbon chemistry of Jupiter family comets and identifying 21P as the prototype of depleted comets (A'Hearn et al. 1995). 21P/G-Z has been observed previously at infrared wavelengths, but a characterization of its volatile composition is far from complete (Weaver et al. 1999; Mumma et al. 2000; DiSanti et al. 2013). We present here the evolution of high-resolution spectra of 21P/GZ acquired as it approached perihelion using iSHELL - the near-IR high resolution immersion echelle spectrograph on NASA/IRTF (Mauna Kea, Hawaii). The individual iSHELL settings cover very wide spectral range with very high accuracy, eliminating many sources of systematic errors when retrieving molecular abundances. We targeted many cometary emission lines across 4 customized instrument settings (L1-c, L3, Lp1-c and M1) in the (2.9 – 5) um range. The bright and peculiar composition of comet 21P/GZ combined with the capabilities of iSHELL provided interesting results. We searched fluorescence emission from HCN, C2H2, water, prompt emission from OH, and many other features in L1-c (2.85 – 3.1 um). Methane, ethane and methanol were targeted both in L3 and Lp1 settings. These species are relevant to astrobiology, owing to questions regarding the origin of pre-biotic organics and water on terrestrial planets. In M1 (near 5um), we targeted multiple ro-vibrational lines of H_2O, CO and the (X-X) system of CN. We will report quantitative abundances for CN and will address its origin by comparing with quantitative production rates for HCN. The ability to quantify both primary and product species eliminates systematic error that may be introduced when measurements are acquired with different astronomical techniques and instruments.

A'Hearn et al. 1995. Icarus 118, 223. DiSanti et al. 2013. ApJ 763:1 (19pp). Mumma et al. 2000. ApJ 531:L155. Weaver et al. 1999. Icarus 142, 482.

Examining Pyrolysis Data from Mars for Evidence of Organic Salts

1C-05
10:15am
W120B

James Lewis (699)

J. L. Eigenbrode (699), A. C. McAdam (699), B. Sutter (JPL), P. D. Archer (JPL), H. B. Franz (698), G. M. Wong (Penn State)

Multiple missions have been sent to Mars with the goal of identifying indigenous organic matter, which could potentially include molecular biosignatures from ancient martian life. These missions have relied on thermal extraction to analyze samples and have so far detected a range of simple aliphatic and aromatic species and ubiquitous carbon dioxide. There are many potential contributors to the observed carbon dioxide and they include the combustion and decarboxylation of organic matter. Understanding the different carbon dioxide profiles that different organic species can generate is therefore of great importance when interpreting

Mars data. Metastable organic salts, such as oxalates and acetates, have been proposed to be widespread on Mars due to the powerful oxidants present on the planet's surface. However, they are challenging to identify using thermal extraction and their detection is further complicated by the presence of perchlorate salts on Mars, which can generate oxidizing conditions in thermal extraction ovens. A range of synthetic oxalate and acetate species were analyzed using a laboratory pyrolysis method analogous to the evolved gas analysis (EGA) experiments being conducted by the Sample Analysis at Mars (SAM) instrument suite on board Curiosity rover. EGA profiles for the species released during pyrolysis of the organic salts on their own were generally not a good match for SAM data. However, when the organic salts were mixed with perchlorates their EGA profiles matched well with flight EGA data. Metastable organic salts mixed with perchlorates may be responsible for many of the carbon dioxide peaks observed by Mars missions.

1C-03
9:45am
W120B

Structural and compositional changes in the upper atmosphere related to the PEDE-2018a dust event on Mars

Meredith Elrod (699)

Stephen Bougher (University of Michigan), Kali Roeten (University of Michigan), Mehdi Benna (699), Paul Mahaffy (699)

The onset of the planet encircling dust event (PEDE-2018a) started 30 May 2018 as observed by MRO/MARCI. After the onset of the event the upper atmosphere underwent structural, compositional, ionospheric, and temperature changes. The Mars Atmosphere and Volatiles EvolutioN (MAVEN) Neutral Gas and Ion Mass Spectrometer (NGIMS) had a good opportunity to observe the dramatic changes in the upper atmosphere including several wind scans from the onset and through the duration of the PEDE. At the onset of the dust even the atmosphere experienced an increase in the variability in the density and temperature profiles across all longitudes or latitudes. Additionally, the structure of the atmosphere exhibits significantly more turbulence after the onset of the dust event across all longitudes causing high variability in the altitude vs density as much as a factor of 5 -10 within a scale height. These significant structural features in the upper atmosphere made for dramatic variations not only the total density as measured by the navigation and accelerometer, but also in the specific neutral and ion compositions. Additionally, ion densities decreased over this period. We intend to map these structural and compositional changes as related to the dust event.

Mars Science Laboratory Observations of the 2018/Mars Year 34 Global Dust Storm

1C-04
10:00am
W120B

Scott Guzewich (693)

M. Lemmon, G. Martinez, A. de Vicente-Retortillo, C.E. Newman, M. Baker, C. Campbell, B. Cooper, J. Crisp, J. Gomez-Elvira, A.-M. Harri, D. Hassler, F. J. Martin-Torres, T. McConnochie, J.E. Moores, H. Kahanpaa, A. Khayat (693), C.L. Smith, M.D. Smith (693), R. Sullivan, M. de la Torre Juarez, A. Vasavada, D. Videz-Moreiras, C. Zeitlin, Maria-Paz Zorzano Mier

Observations of the 2018/Mars Year 34 global dust storm by the Mars Science Laboratory Curiosity rover provide the most comprehensive in situ meteorological and environmental measurements ever recorded during a martian global dust storm, enhancing measurements taken by the Viking landers and Mars Exploration Rovers during the 1977/Mars Year 12 and 2007/Mars Year 28 global dust storms, respectively. The storm saw a drastic reduction in the amplitude of diurnal air and ground temperature variations and a dramatic increase in the amplitude of the semidiurnal pressure tide. Observed dust devil activity within Gale Crater ceased and particular patterns of airfall dust deposition were observed on the rover body.

As the storm developed in the northern hemisphere and near the Mars Exploration Rover Opportunity's landing site, Meridiani Planum, atmospheric opacity in Gale Crater was unseasonably low with a value of 0.57 (measured at a wavelength of 880 nm) at Ls = 188.3° (MSL mission Sol 2073). On MSL mission Sol 2075, the MSL science team initiated a global dust storm science campaign involving a substantially increased cadence of environmental monitoring using the rover's instruments (specifically the frequency of 1-hour duration "extended blocks" with the Rover Environmental Monitoring System and measurements of atmospheric dust levels using the Mast Camera and Navigation Cameras). By Ls = 195.5° (MSL mission Sol 2085) the atmospheric opacity reached 8.5. Due to Curiosity's radioisotope thermoelectric generator power source, science operations were not precluded by the storm.

In this work we present an overview of results from the Curiosity rover during the dust storm. Specific topics discussed include the local and global meteorological conditions, the atmospheric dust opacity variation in both the vertical column and within Gale Crater itself, dust particle properties, aeolian processes during the storm, and the radiation environment.

Session 2A: Planetary Geophysics

Session chairs: Erwan Mazarico & Joe Munchak

2A-01
10:45am
W150

Composition and Surface Properties of the Apennine Bench Formation

Sarah Valencia (698)

Noah Petro (698), Brad Jolliff (Washington University in Saint Louis)

The Apennine Bench Formation (ABF) is a hilly unit between the 2nd and 3rd rings in SE Imbrium Basin on the Moon. The ABF has moderate albedo and was first interpreted as a volcanic unit [1-4]. Due to occurrence near, or at, the Apollo 15 site, it has been argued that the ABF is represented in the Apollo 15 samples in the form of KREEP basalts [e.g. 2-4]. This work will interpret the surface properties and composition of the ABF within the context of the surrounding geologic units in order to further study KREEP basalts on the lunar surface and their link to the Apollo 15 site and samples. This work synthesizes data from orbital lunar missions (i.e., Clementine, Lunar Prospector, Lunar Reconnaissance Orbiter, and Kaguya) to approach studying the ABF with a variety of instrumentation and the highest resolution data available. Analyses include bulk chemistry, topography, terrain ruggedness index (TRI, a unitless measure of surface topographic heterogeneity), and mineralogy. This work finds that the ABF is readily distinguished from nearby mare basalts and crater ejecta units when considering both surface properties of the ABF and bulk chemistry. For example, the ABF is low in estimated FeO (12.3 wt.%) compared to nearby mare (16.9 wt.%), and boundaries are typically sharp. However, the ABF FeO concentration is indistinguishable from the surrounding ejecta, primarily from Archimedes crater, (12.4 wt.% FeO). Additionally, the TRI is useful in distinguishing crater ejecta and ABF, as ejecta deposits are significantly more rugged than ABF (TRI of 1115 vs. 300 respectively). TRI is also used to distinguish between ABF and mare, as mare units are consistently less rugged (TRI averages 130) than ABF. Chemically, the ABF is similar to KREEP basalt samples [3,4]. The ABF has an average FeO of 12.3 wt.% (range = 9.9 – 13.9 wt.%), similar to typical KREEP basalt (average = 11.7 ± 2.5 [6]). Additionally, the ABF is a Th hot-spot, with Th values reaching over 12 ppm (deconvolution done by [5]), again similar to KREEP basalts, whereas ejecta from the surrounding impact craters averages 9.6 ppm Th. Lower concentrations of Th on some regions of the ABF may be owing to lateral mixing of surface material. Volcanic landforms (i.e. vents) on the ABF, located using LROC NAC imagery, support a volcanic origin for the ABF.

[1] Hackman 1966. [2] Hawke B. R., and Head. J. W. (1978) 9th LPSC, 3285-3309. [3] Blewett D. T., and Hawke B. R. (2001) MAPS 36, 701-730. [4] Taylor G. J., et al. (2012) MAPS 47, 861-879. [5] Lawrence D. J., et al. (1999) GRL 26, 2681-2684. [6] New Views of the Moon (2009) Ed. B. L. Jolliff.

Subsurface Structure of Mid-Latitude Glaciers and Icy Dust on Mars

2A-02
11:00am
W150

David Hollibaugh Baker (690.1)

Lynn M. Carter (University of Arizona), Gareth Morgan (Planetary Science Institute)

The mid-latitudes (0-50°) of Mars are host to landforms involving substantial quantities of ice. These landforms include features interpreted to be debris-covered glaciers that are hundreds of meters in thickness and icy dust deposits, or "mantles," that are tens to over a hundred meters in thickness. Understanding their subsurface structure and spatial distribution, including ice and debris content, is important for constraining past climate and volatile exchange. It is also important for assessing the accessibility of ice for future robotic and human exploration. Here we use high-resolution imaging and digital elevation models to assess the characteristics of small impact craters formed within ice-rich features. Craters can be used as natural probes to investigate subsurface ice content, thicknesses, and density contrasts. We also use radar sounding data from the SHAllow RADar (SHARAD) instrument to constrain the dielectric properties and thicknesses of the deposits. The shallow subsurface (<50 m) of martian debris-covered glaciers consists of ice-dust mantle deposits on top of boulder-rich rockfall, with little internal strength variations. Radar data of the glaciers reveal low radar loss and basal reflectors with high power that imply nearly pure (>80%) water ice throughout most of their depth. Nearby mantle units have basal radar reflectors at average two-way time delays of 1.2 μs that are interpreted to be the contact with underlying volcanic plains. Topography constrains the thickness to be ∼100 m, with real dielectric constants of ∼5.0, consistent with ∼50-70% debris and 30-50% ice/pore space. In other mantled areas, deeper radar reflectors (average two-way time delays of 4.2 μs) are continuous with glacial basal reflectors and suggest lower bulk dielectric constants of ∼4.5. The power and time delays of these reflectors imply a thick (∼150-200 m) mantle/debris layer on top of pure glacial ice, or a mixture of debris and ice throughout the ∼300 m depth. These results indicate that there are variations in ice content and structure of mantle units in the mid-latitudes of Mars that should be further investigated by future radar and geomorphic investigations.

A Bernese gravity field of the Moon and an overview on Swiss activities in planetary geodesy

2A-03
11:15am
W150

Stefano Bertone (698)

Daniel Arnold (AIUB), Adrian Jäggi (AIUB), Valre Girardin (AIUB), Alireza Hosseini (WP Unibe), William Desprats (CNES), Jayraj Inamdar (AIUB)

The Astronomical Institute of the University of Bern (AIUB), Switzerland, is still a rather new player in the field of planetary geodesy and orbit determination using deep-space radiotracking data. Nevertheless, our latest developments in the in-house Bernese GNSS Software (BSW) and the experience gained with the processing of GRAIL data opened the way to many research and collaboration opportunities. In this presentation we mainly discuss our latest GRAIL-based lunar gravity fields generated with the Celestial Mechanics

Approach using the planetary extension of the BSW. Based on one-way X band and two-way S-band Doppler data, we perform orbit determination by solving six initial orbital elements, dynamical parameters, and stochastic parameters in daily arcs using a least-squares adjustment. Significative improvements to our solutions come from the recent implementation of an accurate modeling of non-gravitational forces, including accelerations due to solar and planetary (albedo and IR) radiation pressure, based on the 28-plate macromodel to represent the GRAIL satellites. Empirical and pseudo-stochastic parameters are estimated on top of our dynamical modeling to absorb its deficiencies. We analyze the impact of different parametrizations using either pulses (i.e., instantaneous velocity changes) and piecewise constant accelerations (PCA) on our orbits. Based on these improved orbits, one- and two-way Doppler and KBRR data are then used together with an appropriate weighting for a combined orbit and gravity field determination process. We present our latest solutions of the lunar gravity field, based on the recent GRAIL GRGM900C gravity field (as validation of our modeling and parametrization) and on iterations from the SELENE SGM150J gravity field (to check the independence of our solution). We detail our procedure to gradually enlarge the parameter space while adding new data to our gravity field solution and we compare all of our results with the most recent solutions of the lunar gravity field and of other geodetic parameters released by other groups. Finally, we give an overview on currently ongoing projects, including closed-loop simulations of BepiColombo Mercury Planetary Orbiter (MPO) Doppler and altimetry data, non-gravitational force modeling for the re-analysis of Magellan orbit at Venus, and our contributions to the Joint Europa Mission (JEM) proposal.

Geodetic Evidence that Mercury has a Large Solid Inner Core

2A-04
11:30am
W150

Antonio Genova (698)

Sander Goossens (698), Erwan Mazarico (698), Frank G. Lemoine (61A), Gregory A. Neumann (698), Weijia Kuang (61A), Terence J. Sabaka (61A), David E. Smith (MIT), Maria T. Zuber (MIT)

The MErcury Surface, Space ENvironment, GEochemistry, and Ranging (MESSENGER) mission addressed key scientific objectives focused on the interior of the planet with dedicated magnetic and gravity investigations. One of the main questions that is still unanswered concerns the mass distribution within the different layers of the planet interior and, in particular, nature and size of the solid inner core. The analysis of the entire MESSENGER radio science dataset, which includes the low-altitude campaign, enabled us to substantially improve the knowledge of Mercury's gravity field and obliquity of the spin axis. These geophysical quantities are necessary to refine the polar moment of inertia of the whole planet, which bears on the level of differentiation. Our new gravity solution provides refined estimates of the spin axis coordinates (right ascension and declination) that led us to estimate accurately the normalized polar moment of inertia. We implemented a Markov-chain Monte Carlo (MCMC) algorithm to obtain solutions that match bulk density and radius and our latest estimates of the normalized polar moment of inertia, and the fractional polar moment

of inertia, which relies on the obliquity of the spin axis and the amplitude of the longitudinal physical librations that was measured by means of Earth-radar observations and MESSENGER imaging and altimetric data. Our new measurements of the polar moments of inertia of the whole planet and of the outer layers (crust+mantle) suggest a more differentiated internal structure for Mercury. These geophysical quantities improve the constraint on the size of the solid inner core with a radius between 0.3 and 0.6 that of the entire core. Furthermore, simulations of Mercury's magnetic field dynamo confirm that the presence of an inner core not larger than half the size of the outer core is consistent with a magnetic field, thus providing an additional constraint on the size of the solid inner core.

Development of a Mars Lidar (MARLI) for Measuring Wind and Aerosol Profiles from Orbit

2A-05
11:45am
W150

Daniel Cremons (698)

James Abshire (690), Graham Allan (614), Xiaoli Sun (698), Haris Riris (614), Michael Smith (693), Scott Guzewich (693), Anthony Yu (554)

Our understanding of the Mars atmosphere and the coupled atmospheric processes that drive its seasonal cycles is limited by a lack of observational data, particularly measurements that capture diurnal and seasonal variations on a global scale. As outlined in the 2011 Planetary Science Decadal Survey and the recent Mars Exploration Program Analysis Group (MEPAG) Goals Document, near-polar-orbital measurements of height-resolved aerosol backscatter and wind profiles are a high-priority for the scientific community and would be valuable science products as part of a next-generation orbital science package. To address these needs, we have designed and tested a breadboard version of a direct detection atmospheric wind lidar for Mars orbit. It uses a single-frequency, seeded Nd:YAG laser ring oscillator operating at 1064 nm (4 kHz repetition rate), with a 30-ns pulse duration amplified to 4 mJ pulse energy. The receiver uses a Fabry-Perot etalon as part of a dual-edge optical discrimination technique to isolate the Doppler-induced frequency shift of the backscattered photons. To detect weak aerosol backscatter profiles, the instrument uses a 4x4 photon-counting HgCdTe APD detector with a 7 MHz bandwidth and < 0.4 fW/Hz$^{1/2}$ noise equivalent power. With the MARLI lidar breadboard instrument, we were able to measure Doppler shifts continuously between 1 and 30 m/s by using a rotating chopper wheel to impart a Doppler shift to incident laser pulses. We then coupled the transmitter and receiver systems to a laser ranging telescope at the Goddard Geophysical and Astronomical Observatory (GGAO) to measure backscatter and Doppler wind profiles in the atmosphere from the ground. We measured a 5.3 ± 0.8 m/s wind speed from clouds in the planetary boundary layer at a range of 4 to 6 km. This measurement was confirmed with a range-over-time measurement to the same clouds as well as compared to EMC meteorological models. Here we describe the lidar approach and the breadboard instrument, and report some early results from ongoing field experiments.

Session 2B: Galaxies and Cosmology

Session chairs: Knicole Colon & Greg Mosby

Clustering Properties of Emission Line Selected Galaxies over the past 12.5 Gyrs

2B-01
10:45am
W120A

Ali Ahmad Khostovan (661)

David Sobral, Bahram Mobasher, Philip N. Best, Ian Smail, Jorryt Matthee, Behnam Darvish, Hooshang Nayyeri, Shoubaneh Hemmati, John P. Stott

I will present my latest results on the clustering and halo properties of star-forming galaxies selected from the High-z Emission Line Survey (HiZELS) and the Slicing COSMOS 4K (SC4K) narrowband surveys. Our samples consists of ∼7000 [OIII] and [OII] emission line galaxies from HiZELS between z ∼ 0.8 and 4.7 separated in 4 discrete redshift slices, respectively, and ∼4000 Lyα emitters between z ∼ 2.5 and 5.8 separated in 15 redshift slices. I will begin this talk by briefly describing the past work that has been done with these samples as motivation to study clustering/halo properties. My talk will focus on our findings regarding the correlations between halo mass and the physical properties of star-forming galaxies (e.g., line luminosity, stellar mass, star formation rates). For the [OIII] and [OII] samples, I find strongly increasing and redshift-independent trends between line luminosity and halo mass with evidence for a shallower slope at the bright-end consistent with halo masses of $\sim 10^{12.5-13}$ $M_{\odot}$. Similar, but weaker, trends between stellar mass and halo mass have also been found. I investigate the inter-dependencies of these trends on halo mass and find that the correlation with line luminosity is stronger than with stellar mass. This suggest that active galaxies may be connected with their host DMHs simply based on their emission line luminosity. I will also present my most recent results using the SC4K Lyα emitter samples, where I find similar trends to that seen with the [OIII] and [OII] samples, as well as previous Hα measurements, which suggests emission line-selected galaxies may be tracing the same subpopulation of star forming galaxies. I will conclude my talk with an interpretation of this connection and suggest that the shallower slope seen for the brightest emitters is evidence for a transitional halo mass as suggested in models where quenching mechanisms truncate star formation activity and reduce the fraction of star forming galaxies with increasing halo mass.

Gauging the Power of AGN Feedback

2B-02
11:00am
W120A

Travis C. Fischer (665)

Active galactic nuclei (AGNs) are powered by the accretion of matter onto a supermassive black hole (SMBH), which generates massive amounts of radiation within a very small volume. Mass outflows of ionized gas are also generated and have been thought to be critical in galaxy evolution scenarios, where ignition of the AGN quenches star formation and evacuates gas from the stellar bulge. However, recent spatially-resolved kinematic studies of ionized gas in the narrow-line regions (NLRs) of nearby Seyferts and quasars have shown that outflows scale with luminosity but, over the luminosity range sampled, fail to extend further than $\sim$1-2 kpc from the central engine. I will discuss ongoing multiwavelength investigations on the properties of AGN feedback in order to determine the effectiveness of AGN to clear material from their host bulges and significantly affect star formation rates in the nearby universe.

Active galactic nuclei in multi-messenger era

2B-03
11:15am
W120A

Bindu Rani (661)

Feeding on the surrounding gas at the centers of active galactic nuclei (AGN), supermassive black holes often produce collimated outflows, known as relativistic jets, whose tightly collimated beams of radiation pierce through the Universe and reach us from billions of years in the past, offering a unique opportunity to study the Universe when it was an order of magnitude younger than today. An exciting discovery made by space- and ground-based high-energy missions is the detection of gamma-rays from over 5000 AGN. Despite the intensive study of AGN, the location and origin of gamma-rays remains a mystery. Multi-frequency observations offer an unparalleled opportunity to probe and pinpoint the high-energy emission. I will present some exciting results of our recent study using multi-frequency and multi-messenger observations and our plans for the future high-energy missions.

Extracting gravitational-wave sources from incomplete listening sessions with LISA

2B-04
11:30am
W120A

Quentin Baghi (663)

Ira Thorpe (663), Jacob Slutsky (663), John Baker (663), Tito Dal Canton (663)

The future space-based gravitational-wave observatory LISA will be able to detect tens of thousands of astrophysical sources by listening to gravity in the low frequency band, between 0.1 mHz to 1 Hz. From cosmic dawn to the present, LISA will probe a wide range of objects from black hole seeds and massive black hole binaries to ultra-compact binaries in the Milky Way. The detection and characterization of all resolvable sources is a challenge in itself, but we foresee that the data analysis will be further complicated by interruptions occurring in the interferometric measurements. These interruptions will be due to various causes such as laser frequency switches (from days to weeks), high-gain antenna re-pointing (every 2 weeks) and orbit corrections (every month), or unplanned random events. Extracting long-lasting gravitational-wave sources from gapped data raise problems such as noise leakage and computational difficulties. We address these issues by developing a Bayesian method that reintroduces the missing data as auxiliary variables in the sampling of the posterior distribution of astrophysical parameters, which dramatically improves the sampling efficiency and cancels leakage effects. We apply the method to the estimation of galactic binaries parameters, with different gap patterns, and we compare the results to the case of complete data.

Nimble: A Mission Concept for Gravitational Wave Counterpart Astrophysics

2B-05
11:45am
W120A

Joshua Schlieder (667)

Judith Racusin (661), Thomas Barclay (667), Brad Cenko (661), Maxime Rizzo (667), Sarah Logsdon (667), Qian Gong (550), Julie McEnery (661), Jeremy Perkins (661), Kimberly Weaver (662), Stephen Rinehart (665), Eric Lopez (693), Michael McElwain (667), Padi Boyd (667)

In August 2017, the first detection of a gravitational wave event from merging neutron stars coincident with a short gamma-ray burst (sGRB) triggered a world-wide observing campaign to identify and characterize the associated kilonova emission. This event led to numerous firsts and discoveries that began to unveil the mysteries of these energetic astronomical phenomena. However, many questions remain and the field of multimessenger astrophysics is prime for further discovery. Here we describe Nimble, a NASA Explorer class mission concept that couples a very wide-field gamma ray monitor with a UV-Optical-IR telescope and rapid response spacecraft to enable the prompt detection and localization of sGRBs and follow-up of kilonovae. We will describe the science drivers for Nimble and detail the current engineering concept. Nimble will reveal the nature of neutron star merger multimessenger events and its flexible platform will allow for a wide range of additional multiwavelength time domain science.

Session 2C: Air Quality

Session chairs: Ed Nowottnick & Manuela Girotto

Direct Observations of Pollution Gradients Within the Chesapeake Bay Watershed: Overview of the OWLETS-2 Study

2C-01
10:45am
W120B

John Sullivan (614)

John Sullivan (614), Tim Berkoff, Joel Dreessen, Ruben Delgado, Guillaume Gronoff, Lance Nino, Brian Carroll, Vanessa Caceido, Laura Judd, Jay Al-Saadi, Maria Tzortziou, Vernon Morris, Chris Hennigan, Stephan De Wekker, Misti Zamora, Ricardo Sakai, Adrian Flores, Xinrong Ren, Russell Dickerson, Phil Stratton, Winston Luke, Sean Flynn, William Shuart, Reem Hannun (614), Grant Sumnicht (614), Larry Twigg (614), Natasha Dacic (614), Belay Demoz, Bob Swap (614), Thomas McGee (614)

One of the major difficulties for the modeling and satellite communities is the validation of O_3 levels in sharp coastal transition regions within metropolitan areas. Land-water gradients in pollutants can be significant due to differences in emissions (and specific O_3 precursors), surface deposition, boundary layer height, and cloud coverage. The Ozone Water-Land Environmental Transition Study (OWLETS-2), was a follow-on field campaign conducted in the summer 2018 within the Upper Chesapeake region to better characterize spatial and vertical distribution of pollutants across the coastal boundary. To quantify these gradients, research instrumentation was deployed directly within the marine environment (Hart Miller Island, HMI) and at a several continental sites (University of Maryland, Baltimore County (UMBC), Howard U.' Beltsville (HUBV)). Regulatory sites within Maryland, operated by the Maryland Department of the Environment (MDE), were also utilized to better characterize pollution levels within the region. During intensive measurement days, time-synchronized data were collected from ground-based measurements, which included: TOLNet lidars, micro-pulse lidars, ceilometers, radiometers, Doppler wind lidars, ozonesondes, O_3 sensors mounted on mobile platforms (including UAV), Pandora, AERONet, and a diverse set of in situ chemical (trace gas and particulate) measurements. To better infer gradients between the research sites and to provide context for regional analyses, two aircraft and research vessels also contributed to OWLETS-2 as various points during the campaign: the NASA Langley Falcon with the GeoTASO passive remote sensor, the UMD Cessna with an in-situ chemistry analysis suite, and several research vessels with both remote and in-situ sensors. These observations, coupled with reliable chemical transport simulations, are expected to lead to a more fully characterized and complete land-water interaction observing system that can be used to assess future geostationary air quality instruments, such as the NASA Tropospheric Emissions: Monitoring of Pollution (TEMPO) as well as current low earth orbiting instruments such as the European Space Agency's Sentinel 5-Precursor (S5-P) with its Tropospheric Monitoring Instrument (TROPOMI).

Comparison and spatiotemporal analysis of ozone from Pandora, ozonesonde and ozone lidar measurements during OWLETS

2C-02
11:00am
W120B

Alexander Kotsakis (614)

Alexander Kotsakis (614), Joseph Robinson (614), John Sullivan (614), Timothy Berkoff (614), Travis N Knepp (614), Guillaume Gronoff (614), Alexander Cede (GESTAR) and Robert Swap (614)

Pandora has long been compared and validated against satellite and other ground remote sensing instrumentation. However, recent advancements in both Pandora and active remote sensing platforms require additional comparisons and validation. Coupling this with in-situ measurements of ozone creates a strong vertically resolved dataset that can additionally be used in tracking ozone variability. In anticipation of geostationary air quality missions, understanding sub-pixel tropospheric ozone variability from ground-based remote sensing and complimentary measurement platforms will be needed for proper analysis of future retrievals. OWLETS (July-August 2017) investigated the southern Chesapeake Bay to better understand the variability of ozone and other trace gases spatiotemporally over the land-water interface. Comparisons and validation of columnar ozone are made using observations from Pandora spectrometers, ozonesondes, ozone lidars, and other complementary measurement platforms. Further, evaluation of diurnal column ozone behavior in different air quality regimes is presented using the high temporal resolution of Pandora measurements relative to other remote sensing methods. The results of this study will show the variability in tropospheric ozone spatiotemporally and relative to other measurement methods.

Using NASA's new composition forecast to investigate ozone exceedance events linked with stratospheric intrusions

2C-03
11:15am
W120B

K. Emma Knowland (610.1)

Christoph Keller (610.1), Lesley Ott (610.1), Bryan Duncan (614), Krzysztof Wargan (610.1)

Stratospheric intrusions – the introduction of ozone-rich stratospheric air into the troposphere – are well known to negatively influence surface ozone air quality, especially at the high elevations in the western USA in springtime. Simulating and predicting such events remains challenging, as stratospheric intrusions are fine-scale features which require the resolution to be high enough to capture these filaments ($<$ 50 km in horizontal). In addition, the EPA lowered the U.S. national ambient air quality standard for daily maximum 8-hour average (MDA8) ozone, which stresses the need for more rapid identification of the impact of stratospheric air on surface ozone concentrations. An analysis of the stratospheric intrusion-influenced ozone exceedance events over the continental US was performed for the spring seasons of 2017 and 2018 using NASA's new global high-resolution air quality forecasts, "GEOS-CF". Forecasting air quality has typically been performed at the local-scale, either for an individual city, state or country. The NASA's Goddard Earth Observing System (GEOS) model has been expanded to provide global near-real-time forecasts of atmospheric composition, GEOS-CF, at the high horizontal resolution of 0.25 degrees ($\sim$25 km). This

system combines the operational GEOS weather forecasting model with the state-of-the-science GEOS-Chem chemistry module (version 11) to provide detailed chemical analysis of a wide range of air pollutants including ozone, carbon monoxide, nitrogen oxides, and fine particulate matter (PM2.5). The resolution of the GEOS-CF forecasts is the highest resolution compared to current publicly-available global composition forecasts. A suite of observational datasets and model products are used in the analysis of the events, with a focus on forecast skill. This analysis demonstrates that our operational analyses may aid in forecasting such events, providing useful diagnostics to air quality managers.

Global Modeling Assessment of PM2.5 During Wildfires: Inferring the Impact of PM2.5 Exposure on Adverse Respiratory

2C-04
11:30am
W120B

Emily Saunders (610.1)

Christoph A. Keller (610.1), K. Emma Knowland (610.1), Steven Pawson (610.1)

Particulate matter pollution is a mixture of solid and liquid droplets floating in the air that can lead to reduced air quality and increased adverse health impact. Fine particulate matter (PM2.5) can be emitted into the air from anthropogenic sources such as the burning of fossil fuels, motor vehicles, and power plant emissions. Exposure to PM2.5 can aggravate pre-existing respiratory and cardiovascular conditions. When PM2.5 is inhaled it can cause damage to the lungs such as reduced lung function and shortness of breath. After being inhaled PM2.5 can enter the bloodstream and cause harm to the heart. One major natural source of PM2.5 exposure is from wildfire smoke. The particulates within the smoke from the wildfires can spread from the initial source region, potentially impacting communities both near and far. During and after wildfire events, PM2.5 levels can exceed the WHO air quality guidelines (10 μg/m^3 annual mean; 25 μg/m^3 daily mean), becoming hazardous to an individual's health. Global models can be used to simulate the emission and transport of these particulates and subsequently they can be valuable to air quality forecasting in highly polluted areas. The NASA Goddard Earth Observing System (GEOS) Composition Forecast (GEOS-CF) system has been used to produce near-real time air quality forecasts of atmospheric composition at a high global resolution of 25x25 km^2. The GEOS-CF system utilizes the GEOS weather forecast model coupled with GEOS-Chem (version 11) chemistry module to provide analyses and forecasts of various toxic air pollutants, including PM2.5. The GEOS-CF simulated high levels of PM2.5 (40 μg/m^{3}o 250 μg/m^3, exceeding the WHO guidelines, during multiple recent regional and global wildfire seasons, including the 2017 Washington State and Northern and Southern California wildfire seasons. Furthermore, the GEOS-CF simulated PM2.5 applied to a human health assessment model, BenMAP (The Environmental Benefits Mapping and Analysis Program, version 1.3), estimates the impact on adverse respiratory health conditions due to PM2.5 exposure from wildfires. The GEOS-CF predicted PM2.5 during the wildfire season with the corresponding BenMAP results provides an assessment of the human health impact of PM2.5 exposure.

A Physical Approach to Constraining CTM PM2.5 Modeling Outputs Using Surface-Monitor Measurements & Satellite Retrievals

2C-05
11:45am
W120B

Mariel Friberg (613)

M D Friberg (613), R A Kahn (613), J A Limbacher (613), K W Appel (EPA), J A Mulholland (Georgia Tech)

Improved satellite retrievals of aerosol type can provide broad regional context and can decrease metric uncertainties and errors, increasing the accuracy of near-surface air quality characterization. The frequent, spatially extensive and radiometrically consistent instantaneous constraints can be especially useful in areas away from ground monitors and progressively downwind of emission sources. We demonstrate a physical approach of using satellite retrievals to further improve regional-scale chemical transport model (CTM) spatiotemporal estimates of PM2.5, its major chemical component species, and its related uncertainties. This approach complements the more widely applied statistical modeling methods. It uses ground-based monitors where available, combined with aerosol optical depth from both the Multi-angle Imaging SpectroRadiometer (MISR) Research Aerosol retrieval algorithm (RA) and Moderate Resolution Imaging Spectroradiometer Multi-Angle Implementation of Atmospheric Correction (MAIAC) advanced algorithm, as well as MISR qualitative constraints on aerosol size, shape, and light-absorption properties. The technique developed here leverages the complete spatiotemporal coverage of CTMs and their physical constraints, such as aerosol mass balance and meteorological consistency. The CTM also aids in identifying relationships between observed species concentrations and emission sources. We examine the optimal application of incorporating 275 m horizontal-resolution aerosol airmass-type maps from the MISR RA and total-column aerosol optical depth from the MISR RA and MAIAC into regional-scale CTM outputs. The impact on surface PM2.5 fields progressively downwind of large single sources will be discussed and evaluated using concurrent ambient air quality observations. Assessing this physical technique in well-instrumented regions opens the possibility of applying it globally over areas where surface air quality measurements are limited or entirely absent.

Session 3A: Understanding Earth and Analogs

Session chairs: Manisha Ganeshan & Erwan Mazarico

Repeat field campaigns at Holuhraun, Iceland: Exploring a new volcanic vent as a planetary surface terrestrial analog

3A-01
12:45pm
W150

Jacob Richardson (698)
Sarah Sutton, Patrick Whelley (698), Stephen Scheidt, Christopher Hamilton, Debra Needham, Jacob Bleacher (698)

Volcanic vents are found on all terrestrial bodies larger than Ceres, where lava, pyroclasts, and gases were erupted onto the surface. The morphology of volcanic vents is indicative of their eruption style, rate, duration, and volume. Vents on all planetary surfaces experience degradation over time, which complicates methods that model eruption characteristics using observed vent morphology. The recent Holuhraun eruption in central Iceland provides an ideal case to observe how volcanic vents age and erode. In 2014 and 2015, the Holuhraun lava field was emplaced as a flood lava, the largest on Iceland since the 1783-4 Laki eruption, covering 85 sq km of land with 1.4 cu km of basalt. Six months after the cessation of lava effusion at the main vent, we surveyed the interior of the vent using a terrestrial scanning lidar positioned with differential GPS. This survey produced a millimeter to decimeter resolved point cloud of the floor and walls of the vent and a drainage channel that developed at its northeast end. We repeated this survey in 2016 and 2018, gathering new point clouds of the now three-year-old vent. This unprecedented time series enables the precise measurement of mass wasting events and other topographic changes at the vent. These include massive blocks 10 m in width that have slumped down the interior walls of the vent and the build up of scree slopes.

Historical Hurricanes in MERRA-2

3A-02
1:00pm
W150

Marangelly Cordero-Fuentes (610.1)
Oreste Reale (610.1)

Tropical cyclones were not detected in global scale analyses until the 1990s. The initialization problem was a major hindrance in hurricane forecasting. Artificial enhancements of the cyclone circulation e.g., the 'bogus vortex', were commonly used, even when initializing multiply-nested regional models at horizontal resolutions which should have allowed for a representation of a hurricane structure. Modern-Era Retrospective Analysis for Research and Applications, version 2 (MERRA-2), offers an unprecedented view of 'historical hurricanes' that occurred in the years between 1979 and 1989. The assimilation of existing observations with a modern data assimilation system reveals that most of the hurricanes observed in

those years can indeed be represented in global analyses. While the tropical cyclone fine structure cannot be solved and intensity is obviously underestimated at the resolution of MERRA-2, a very clear 'signature' of the tropical cyclone with center pressures down to 950 hPa, vertical aligned structure, strong warm core, and wind maxima exceeding 40 m/s can nevertheless be detected, fully consistent with the large-scale environment. Examples from infamous hurricanes such as David (1979), Frederic (1979), Allen (1980), and Elena (1985) will be provided. MERRA-2 provides an enormous improvement not only with respect to operational analyses of the time, but also with respect to contemporary reanalyses, thus establishing a solid starting point for downscaling studies.

Indonesian fire and drought during 1979-2016: Connection with El Niño and Indian Ocean Dipole (IOD)

3A-03
1:15pm
W150

Xiaohua Pan (614)

Mian Chin (614), Charles Ichoku (613), Robert Field (611)

This study advances the previous understanding of the role of climate variability on Indonesian fire activity, by considering (i) the presence of different types of El Niño and (ii) the interaction between El Niño and the Indian Ocean Dipole (IOD). We classify 12 El Niño events during 1979–2016 into Eastern Pacific (EP) and Central Pacific (CP) types (four and eight El Niño events, respectively) and analyze observational data of sea surface temperature, precipitation, drought code, biomass burning carbon emission, visibility, and aerosol optical depth accordingly. We find that more intense and prolonged Indonesian drought and fires occur in the EP type, during which the emitted carbon amounts almost double those in the CP type. By further separating the CP type El Niño according to the phase of the IOD, that is, positive and negative, we show that fire seasons with less burning intensity and shorter duration are predominantly associated with weakly positive or even negative phase of the IOD phenomena. Moreover, fire intensity exhibits geographic diversity: fires are always more intensive in southern Kalimantan than in southern Sumatra in all El Niño events, although it is less dry in the former region. The outcome of this study can be applied to drought early warning, fire management, and air quality forecast in Indonesia and adjacent areas by identifying the type of El Niño and the phase of the IOD in advance.

A new map of forest extent and structure for Trees outside Forest (ToF) in Bangladesh

3A-04
1:30pm
W150

Nathan Thomas (618)

Priscilla Baltezar (Clark University), Temilola Fatoyinbo (618), David Lagomasino (618), Seung-Kuk Lee (618), Justin Green (US Forest Service International Program), Mizanur Rahman (Graduate School of Global Environmental Studies, Kyoto University)

Trees in Bangladesh are disproportionately important. An estimated 11% of Bangladesh is forested and it has one of the lowest forested land per capita (0.009 ha person) estimates globally (FAO., 2015). Approximately 40% of the Bangladesh natural forest area has been lost since 1930 (Reddy et al., 2016) due to demands for wood products and land for agriculture. Trees outside forest (ToF), defined as discrete trees and small groups of trees in non-forest settings, therefore provide important ecosystem services and are an essential socioeconomic and ecological asset. Previous assessments of ToF have often been limited by the unavailability of sufficient high-enough resolution remotely sensed imagery and have primarily utilized optical data only. We have generated a new forest extent map for all trees within Bangladesh. We used a combination of ESA Sentinel-1 and Sentinel-2imagery within the Google Earth Engine environment. Thresholds on Sentinel-1 Synthetic Aperture Radar (SAR) HV-polarization and Sentinel-2 NDVI were used to derive tree extent, at 10 m resolution (mmu >1/8 ha). Tree canopy height at 30 m resolution was generated using a DLR Tandem-X InSar digital surface model (DSM) and associated interpolated digital terrain model (DTM) (RMSE 1.26 m). We mapped 4.5 million ha of trees, increasing existing estimates of tree cover extent, as a consequence of the use of higher resolution multi-modal imagery. We derived country wide canopy height (excluding mountainous terrain) for trees outside of continuous forests (i.e., forested hillsides, mangroves). Further work is oriented towards improving canopy height estimates over sloped terrain and deriving biomass estimations from field collected allometry. We successfully generated a new tree extent and canopy height map that will serve as baseline products for the monitoring of terrestrial carbon within a heavily fragmented yet important forest resource. This work contributes to a USAID SilvaCarbon initiative to facilitate the monitoring of forest extent and terrestrial carbon by the Bangladesh Forest service.

Landslide Hazard and Exposure from Satellite Data - A Case Study in Bangladesh

3A-05
1:45pm
W150

Robert Emberson (617)

Dalia Kirschbaum (617), Thomas Stanley (USRA/617)

Landslides are a key hazard in a range of mountainous landscapes around the world, with significant costs in terms of loss of life and financial outlay every year. At very local field scales, landslide risk and hazard can be estimated based on a range of geotechnical parameters, but the use of satellite data to assess landslide hazard remains limited. The recently released Landslide Hazard Assessment for Situational Awareness (LHASA) model from NASA researchers allows global assessment of qualitative landslide hazard in near real

time based on satellite derived precipitation data and a global susceptibility map, and this 1km resolution model represents an ideal foundation for a global landslide risk model. To enable us to build better models of risk associated with landslides from satellite data, it is necessary to understand the specific situations where populations are most vulnerable to landslide hazard. These situations include during other major natural disasters, such as tropical storms or earthquakes, which can trigger extensive landsliding, or in communities that have specific socio-economic factors that contribute to excess vulnerability. In this contribution, we explore a case study of the latter kind: the Rohingya refugee camps in Bangladesh, where temporary encampments of vulnerable populations are exposed to landslide hazard. We explore how satellite data and openly available socioeconomic data can be used to better quantify the specific risk of landslides and the exposure of infrastructure and population to this threat. Additionally, we report on lessons learned for communication of hazard and risk information to vulnerable communities, since data driven products must be carefully explained and modified to suit end-users and their specific decision making processes.

Session 3B: Ocean and Ice

Session chairs: Greg Mosby & Lauren Andrews

Impacts of improved in-water light calculations for ocean circulation-ecosystem models

3B-01
12:45pm
W120A

Grace Kim (616)

Carlos Del Castillo (616), Antonio Mannino (616)

Accurate representation of light in water is important for modeling ocean and estuarine processes. Sunlight is the primary source of heat for the ocean. Phytoplankton use sunlight to grow, producing oxygen during photosynthesis. In many coupled ocean circulation-ecosystem models, irradiance calculations do not account for light attenuation by materials in the aquatic environment. We investigate the effects of improving the representation of light in a global ocean circulation model and a regional model of the Chesapeake Bay. Model improvements were aided by ocean color satellite data products which provide information about the living and dissolved materials in the water. In our global ocean studies, we find ocean productivity, ice extent and surface ocean heat content are affected by including the light attenuation by dissolved materials. In the Chesapeake Bay, we changed the calculations for in-water solar heating to more realistically simulate light in the coastal environment. This increased vertical stratification, which intensified bottom water oxygen depletion. Implications of expected future increases in riverine flux into estuaries and the ocean will be discussed.

Understanding airborne fertilization of oceanic ecosystems using Satellite and Model data

3B-02
1:00pm
W120A

Yingxi Shi (613)

Toby Westberry, Lorraine Remer, Hongbin Yu (613), Michael Behrenfeld

For a long time, people believe that atmospheric deposition of nutrients fertilizes the ocean ecosystem. To validate this hypothesis, it requires observations on both atmosphere composition and ocean biology in order to understand the pattern and properties of atmosphere deposition and the corresponding ocean response. Using combined satellite data products as well as modeled reanalysis data, we can quantify the deposition frequency and location of transported dust and volcano ash into the ocean. Also a new technique, which utilizes satellite ocean products to detect and distinguish different forms of ocean biology will be used to study ocean responses. As a pilot study, Okmok and Kasatochi 2008 volcano eruptions were chosen, because both eruptions ejected ash rich plumes into the atmosphere and deposited into a nutrient limited ocean area – Alaska bay. We use MODIS observation to track the location and extent of the ash plume and MERRA reanalysis data to confirm the existence and location of the ash deposition. The pattern of volcano ash plumes links to the

satellite observed chlorophyll anomaly, as well as other ocean biology parameters, indicating a basin wide ocean response. This preliminary study is the first step before extending this study globally.

3B-03
1:15pm
W120A

~~Sea state based estimation of white cap fraction: Implications for primary marine aerosol fluxes~~ Withdrawn

Aishwarya Raman (610.1)

Anton S Darmenov (610.1), Shuyi Chen (University of Washington), Milan Curcic (University of Miami), Atanas L Trayanov (610.1)

Oceanic whitecaps (hereafter, W) or the characteristic whiteness of the sea foam is an important feature for predicting exchange of gases, sea spray aerosols (SSAs), heat and momentum transfer between the ocean and the atmosphere at the air-sea interface. Due to its increased surface emission and brightness temperature, whitecaps are critical for satellite retrievals of ocean albedo, ocean color, ocean surface wind vectors from satellite borne radiometer and microwave instruments. Most of the existing models predict W using wind speed and sea surface temperature (SST). However, numerous publications have pointed out that there are large uncertainties in the predicted W and using parameterizations based on wind-wave state can improve the precision of the predicted W. Here, we integrate the University of Miami Wave Model - 2.0 (UMWM) in Goddard Earth Observing System (GEOS) and use wave diagnostics to predict W. We run UMWM/GEOS at 0.5° x 0.5° by replaying to MERRA2 meteorology and evaluate the wave diagnostics using measurements from fixed buoys and satellite altimeters. We use three different parameterizations for W based on: 1) Reynolds number, 2) wave dissipation energy, and 3) volume of air entrained by breaking waves. We compare our results of W with previous studies and also with the satellite based observational dataset. Predicting W is important for understanding the processes at the air-sea interface. Therefore, this work is a step further in improving the uncertainties in the aerosol and atmospheric chemistry modules of the global models.

3B-04
1:30pm
W120A

The Response of Polar Low Intensification to Changing Sea Ice and Sea Surface Temperature

Chelsea L. Parker (615)

Amanda Lynch (Brown University), Priscilla Mooney (Bjerknes Centre for Climate Research, Bergen)

Global climate forcings and polar amplification significantly affect seasonal Arctic sea ice extent, concentration, and thickness. The changing Arctic landscape and climate has important implications for the development of polar low pressure systems. Retreating sea ice, increasing fetch, and increasing sea surface temperatures increase the potential for polar low development, intensification, and trajectory into higher latitudes. However, increasing polar low activity can exacerbate sea ice export from the region, generating a feedback effect. Therefore, understanding the mechanisms of polar low intensification and the interaction

with the ice-ocean interface is critical for understanding the future of polar low activity and Arctic sea ice. However, given a lack of observational data, and the spatio-temporal scale of these systems, the dynamics of polar low intensification remain poorly understood. This study uses numerical weather modeling techniques to provide insight into the life cycle of polar lows. We utilize the National Center for Atmospheric Research (NCAR) Weather Research and Forecasting (WRF) model in a three-domain configuration of 36/12/4 km horizontal grid spacing to simulate polar low events in the Norwegian and Barents Seas (polar low genesis hotspots) between 2011-2015. We analyze the relative contribution of upper level divergence, in-storm convection, and surface level fluxes to the intensification of each simulated polar low. Initial results suggest that while many Barents Sea polar lows are baroclinic and intensify through in-storm convection, several cases demonstrate alternate intensification processes. Our analyses explore the sensitivity of these polar lows to changing sea surface temperatures and sea ice extent and concentration in the model boundary conditions. The analysis focuses on the relative change in the simulated polar low intensification mechanisms and storm characteristics such as pressure, wind speed, precipitation, size, trajectory, and translation speed with the changing environment. Regional, high resolution modeling studies such as these are essential for furthering the understanding of polar low intensification and their sensitivity to the changing climate, and, in turn, the future of Arctic sea ice.

Bed geometry controls response time of Greenland outlet glacier mass loss

3B-05
1:45pm
W120A

Denis Felikson (615)

Ginny Catania (University of Texas at Austin), Mathieu Morlighem (University of California, Irvine), Timothy Bartholomaus (University of Idaho)

The projected contribution to sea-level rise from the Greenland Ice Sheet currently has a large spread in literature, ranging from 14 to 255 mm by the year 2100. Part of this spread is due to uncertainty in mass loss from ocean-terminating outlet glaciers in response to terminus retreat. Here, we use a diffusive-kinematic wave formulation of glacier thinning to show that steep bed features can limit thinning from diffusing inland from a glacier's terminus. This simplified model allows us to rank 141 of Greenland's outlet glaciers based on their potential to allow thinning to diffuse far inland and, thus, contribute to sea-level rise over the next century. We then target two glaciers: Kakivfaat Sermiat (KAK) in West Greenland and Kangerlussuaq Gletscher (KLG) in East Greenland. Both glaciers have a high potential to contribute to sea-level rise but with contrasting bed geometries; KAK has relatively low ice flux but its geometry can allow thinning to diffuse far inland while KLG has high ice flux but a geometry that will limit thinning to 30 km inland of its terminus. We simulate mass loss from each glacier, in response to prescribed terminus retreat, using a higher-order numerical model, and find very different response times of mass loss from the two glaciers over the next century. KLG reaches a new steady state by 2100, while the slow inland diffusion of thinning causes KAK to continue its response into the next century and beyond. As a result, KAK contributes more to sea-level rise than KLG by year 2200, suggesting that low-flux glaciers that can allow thinning to spread far into the ice sheet interior may contribute much to

sea-level rise as high-flux glaciers that limit thinning to their lowest reaches. By identifying the glaciers around the ice sheet with the highest potential to contribute to sea-level rise, we hope to help focus future higher-order numerical modeling studies working toward narrowing the range in sea-level rise projections.

Session 3C: Jupiter and Titan

Session chairs: Erin Dawkins & James Leake

Jupiter's Turbulent Power Spectra from Hubble Space Telescope

3C-01
12:45-1:00pm
W120B

Richard Cosentino (690)
Amy Simon (690), Raul Morales-Juberias

Turbulence in Jupiter's atmosphere was investigated with archival and ongoing observations from the Hubble Space Telescope (HST). Datasets where at least one full rotation (360 degree longitude coverage) taken with the Wide Field Camera instruments (WFPC2 or WFC3) were used to produce a full map of the planet's upper cloud layer. The global maps were analyzed to produce the passive tracer power spectrum of cloud features for single rotation observations. Successive rotations were used to produce the zonal energy power spectrum from winds derived from the observations; an objective of the Outer Planet Atmosphere Legacy (OPAL) program. The turbulent state of the atmosphere's dimensionality and dynamics are reflected in the slopes of such power spectra. The retrieved passive tracer power spectra in Jovian maps has a shallow spectral index over wavenumbers k=1-26. The spectrum transitions to the well-known Kolmogorov $k^{-5/3}$ relation between wavenumbers k=26-40 for small scales up to k=1000. The derived zonal energy power spectra exhibit a $n^{-}5$ relation when selecting a starting meridional wavenumber near k$\sim$26-40. This value matches the number of jets in Jupiter's zonal wind profile and corresponds to the Rhine's scale dynamic quantity. Jupiter's anti-cyclonic and cyclonic shear zones have distinctly different power spectra from each other but when averaged together produce the Kolmogorov $k^{-5/3}$ relation for wavenumbers k=40-1000. Jupiter's atmosphere possesses properties that are consistent with quasi-geostrophic turbulence for shallow fluids which are supported by recent Juno findings on the distribution of ammonia.

Field aligned currents associated with Jupiter's auroras

3C-02
1:00-1:15pm
W120B

Stavros Kotsiaros (695)
J. E. P. Connerney (695), G. Clark, F. Allegrini, G. R. Gladstone, W. S. Kurth, B. H. Mauk, T. K. Greathouse, J. Saur, E. J. Bunce, Y. M. Martos (695), S. J. Bolton, S. M. Levin

The Juno spacecraft has been orbiting Jupiter since July 4, 2016. Juno's 16 - thus far - orbits sampled Jupiter's environment from 1.06 Jovian radii outwards, extending to the distant reaches of the Jovian magnetosphere. Juno's polar orbit makes the first direct observations of the Jovian magnetosphere and auroral emissions from above the poles. We present an extended analysis of Juno's magnetic field obser- vations acquired over the polar regions, revealing magnetic field pertur- bations associated with auroral field aligned (Birkeland) currents. We have assembled a map of the Birkeland currents with contemporaneous ultraviolet spectrometer (UVS) images of the aurora.We compare the magnetic field perturbations with radio and plasma wave data from the Waves instrument as well as with particle

energy data from the Jovian Auroral Distributions Experiment (JADE) and JEDI instruments for a specific event during Juno's traverse of the South auroral oval. We find that the associated field perturbations surprisingly weak (maxi- mum amplitude 200 nT) relative to expectations given Jupiter's in- comparably bright auroras. Moreover, the Birkeland currents appear much more dispersed than would be expected suggesting filamentry structures primarily over the northern polar region.

3C-03
1:15-1:30pm
W120B

Jupiter's magnetic field & Io-related decameter radiation

Yasmina M. Martos (695)
John E.P. Connerney (695), Stavros Kotsiaros (695), Masafumi Imai

The Io-dependent radio emissions from Jupiter ought to originate along magnetic field lines linking Io to the Jovian ionosphere. If these emissions occur at or below the electron gyrofrequency, they ought to be limited in frequency extent by the magnetic field magnitude at the foot of the Io Flux Tube (IFT), a subject of much interest since the 1980's. The lack of agreement between the frequency extent of Io-related decameter radiation and those predicted by Jovian magnetic field models has been hotly debated. In this study we show how the newly proposed magnetic field model (JRM09) can explained these radio emissions. Additionally, the beaming angle of the hollow cone of emission and the altitude of the generation of the decameter radio emissions are estimated and discussed.

3C-04
1:30-1:45pm
W120B

Calculation of high-level ab initio rate constants for key neutral–neutral reactions in low-temperature Titan condition

Shiblee Ratan Barua (693)
Paul Romani (693)

The ultimate source of the complex photochemistry in Titan's upper atmosphere (70–187K) is its background neutral environment which is composed primarily of N_2 and CH_4. Previous photochemical models show that such complex chemistry is strongly influenced by neutral–neutral reactions. Global sensitivity analyses confirm that the large errors associated with the mole fractions of various compounds in the upper atmosphere of Titan originate mainly from the uncertainties in low-temperature rate constants of "key"neutral–neutral reactions. Unfortunately, accurate experimental rate constants for such low-T reactions are difficult, if not impossible, to measure, and the lab data are affected by uncertainties in determining the absolute concentrations of radical species. Currently, the most common theoretical approach involves uncertainty extrapolation technique in which uncertainties in room-temperature rate constants are extrapolated to low-temperature conditions, resulting in large errors in the theoretical low-T rate constant data. To solve this existing problem, we are employing the two-transition-state (2TS) model developed by Klippenstein and coworkers to calculate high-level ab initio rate-constants for key low-T reactions in Titan, and subsequently evaluating the mole fractions using our existing one-dimensional (1D) photochemical model. In particular, we are investigating key reactions that have not yet been

studied in the lab, and for which accurate rate coefficients are still unknown. Our highly accurate theoretical rate constants will be made available to the astrochemistry community at large, and our calculated mole fractions will be used to analyze the Composite Infrared Spectrometer (CIRS) observational data which will vastly improve our current knowledge of the atmosphere of Titan.

Modeling Titan's Coupled Thermosphere and Ionosphere Using a Non Hydrostatic Model

3C-05
1:45-2:00pm
W120B

Jared Bell (675)

Dr. Stephen Bougher (University of Michigan), Dr. J. Hunter Waite (SwRI), Rebecca Perryman (SwRI), Dr. Aaron J. Ridley (UM),

As the Cassini mission has come to a dramatic close, several major questions still remain unanswered. Does Methane escape as suggested by some modeling efforts? What causes the rapidly changing temperatures observed in the neutral densities measured by the Cassini Ion-Neutral Mass Spectrometer (INMS)? To begin to answer these questions with a higher degree of accuracy, the Titan Global Ionosphere-Thermosphere Model (T-GITM), a 3-D non-hydrostatic model of Titan's upper atmosphere, has been developed. In this presentation, we discuss how the newly developed T-GITM compares with in-situ data, we discuss the implications for atmospheric escape from Titan, and we examine the major drivers of the chemistry and energy balance in this moon's upper atmosphere.

Session 4A: Heliophysics

Session chairs: James Leake & Erin Dawkins

4A-01
2:15pm
W150

Multiwavelength Study of 24 Equatorial Coronal-Hole Jets

Pankaj Kumar (674)
Judith T. Karpen, Spiro K. Antiochos, Peter F. Wyper, C. Richard DeVore, Craig E. DeForest

Coronal jets are transient/collimated plasma ejections that repeatedly occur in coronal holes and contribute mass/energy to solar wind and corona. By combining numerical simulations and high-resolution observations, we have made substantial progress recently on determining the energy build-up and release processes in these jets. Here we describe a study of 24 equatorial coronal-hole jets using SDO/AIA and HMI observations on 27-28 June 2013 and 8-10 January 2014. Out of 24 jets, 16 (67%) are associated with mini-filament eruptions and 8 (34%) do not show mini-filament eruptions but do exhibit mini-flare arcades and other CME-like signatures, indicating that every jet in our sample involved a filament-channel eruption. From the complete set of events, 5 jets (21%) are apparently associated with tiny flux-cancellation events at the polarity inversion line, and 3 events are associated with sympathetic eruptions of filaments from neighboring jet sources. Potential field extrapolations of the source regions reveal that almost all jets occurred in the fan-spine topology, and are in agreement with the breakout model of solar eruptions. We present selected examples of each type, and discuss the implications for the jet energy buildup and initiation mechanisms.

4A-02
2:30pm
W150

Observations of Condensations at Coronal Hole Boundaries: Dynamics and Implications

Emily Mason (671)
Spiro Antiochos (670), Aleida Higginson (JHU APL)

Two of the outstanding challenges in Heliophysics are determining the mechanism responsible for heating the corona and determining the origin of the slow solar wind. Physical insight and critical constraints on these problems can be obtained by observing the structure and dynamics of coronal plasma, especially the plasma near the boundary between open and closed magnetic flux. We present recent observations from SDO AIA and IRIS of coronal rain in small null-point topologies that frequently result from decayed active regions near coronal hole boundaries. Coronal rain is the intriguing phenomenon in which plasma at coronal temperatures undergoes rapid cooling (from roughly 10^6 to 10^3 K), condenses, and falls to the surface. Its origins are not thoroughly understood, but proposed theories posit mechanisms of either temporal or spatial variations in coronal heating. Consequently, our quantitative measurements of coronal rain dynamics place important constraints on the properties of coronal heating. Furthermore, our observations clearly show condensation formation at the

open-closed boundary, where interchange reconnection is widely believed to release the slow solar wind. Since these null-point topologies are common features in and near coronal holes, they are ideal targets for the increased temporal and spatial resolution of upcoming solar missions. We will present models for how these condensations form via interchange reconnection and thermal nonequilibrium, and make predictions as to the signatures that Parker Solar Probe and Solar Orbiter will be able to detect.

Data mining for vortices on the Earth's magnetosphere - algorithm application for detection and analysis

4A-03
2:45pm
W150

Yaireska M. Collado-Vega (674)

Virginia L. Kalb (619), David G. Sibeck (674), Kyoung-Joo Hwang (SwRI), Lutz Rastätter (674)

Unsteady processes in the solar wind-agnetosphere interaction, such as vortices developed at the magnetopause boundary by the Kelvin-Helmholtz instability, may contribute to the process of mass, momentum and energy transfer into the Earth's magnetosphere. The research described in this paper validates an algorithm to automatically detect and characterize vortices based on velocity data from simulations. The vortex identification algorithm (VIA) systematically searches the 3-D velocity fields to identify critical points where the magnitude of the velocity vector vanishes. The velocity gradient tensor is computed and its invariants are used to assess vortex structure in the flow field. We use the Community Coordinated Modeling Center (CCMC) Runs on Request capability to create a series of model runs initialized from the conditions observed by the Cluster mission in the Hwang et al. (2011) analysis of Kelvin-Helmholtz vortices observed during southward interplanetary magnetic field (IMF) conditions. We analyze further the properties of the vortices found in the runs, including the velocity changes within their motion across the magnetosheath. We also demonstrate the potential of our tool to identify and characterize other transient features (e.g., flux transfer events, FTEs) with vortical internal structures. We find that the vortices are associated with flows on the magnetosheath side of the magnetopause that reach speeds greater than the solar wind speed at the bow shock.

4A-04
3:00pm
W150

Sounding Rocket Systems Engineering Mission Design: From Concept to Proposal

Sophia Zaccarine (675)
Douglas Rowland (675)

VISIONS and VISIONS-2 are sounding rocket missions with the goal of analyzing the auroral wind and cusp ion outflow using low energy neutral atom (ENA) imaging at low altitudes of the ionosphere. VISIONS-1 launched February 2013 and VISIONS-2 will launch in December 2018. VISIONS-3 is the proposed follow-up mission to VISIONS-1 and VISIONS-2, intended to use tomographic reconstruction with two launch vehicles. The overlap of line-of-sight regions from the two viewpoints of the sounding rockets provides boundary conditions to mathematically constrain data analysis, similar to a CAT Scan. Trade studies were conducted to analyze the benefits of different launch ranges, configurations, number of launch vehicles, type of launch vehicle, number of scientific instruments, mechanical sizing of payload, and their respective effects on the cost of the mission. These trade studies were conducted using a combination of Microsoft Powerpoint, Excel, and Solidworks software. A mass budget constrained by the desired altitude of >650km and a monetary budget capped at 2 million were also considered during these trade studies. The Norway launch range was selected for the launch, with two Black Brant XII Sounding Rockets from Wallops Flight Facility launched between 1-3 minutes apart with a launch azimuth separation of 6-16 degree. The launch will be during the day to analyze the poleward moving auroral forms. Data simulation for the rocket is being done in MATLAB. Goal of model is to accurately predict how many ENA's can be read in for any tumbling rocket configuration, in order to determine optimal rocket configuration and predict measurements for the mission. Future goals for this project include completing the data simulation, defining instrument accommodation requirements, and writing the mission proposal to be submitted to NASA.

Session 4B: The Water Cycle

Session chairs: Joe Munchak & Manisha Ganeshan

Improving GPM Passive Microwave Precipitation over Land Surfaces

4B-01
2:15pm
W120A

Sarah Ringerud (612)
Christa Peters-Lidard (610), Yalei You (UMD-ESSIC), Chris Kummerow (CSU)

Accurate, physically-based precipitation retrieval over global land surfaces is an important goal of the NASA Global Precipitation Measurement Mission (GPM). This is a difficult problem, as the signal over radiometrically warm land surfaces in the microwave frequencies means that the measurements used are indirect, and typically require inferring some type of relationship between an observed scattering signal and precipitation at the surface. GPM, with collocated radiometer and dual-frequency radar, along with a constellation of partner radiometers, is an excellent tool for tackling this problem and improving global retrievals. In the years following the launch of the GPM core satellite, physically-based passive microwave retrieval of precipitation over land continues to be challenging. In this work, it is demonstrated that the operational GPM passive microwave algorithm, the Goddard Profiling Alogorithm (GPROF) tends to overestimate precipitation at the low (< 5 mm/hr) end, and underestimate at the high end (> 10 mm/hr) of the distribution over land. Retrieval sensitivities to dynamic surface conditions are explored using instantaneous retrievals of surface emissivity and associated soil and vegetation characteristics. Through the addition of this information, along with improvements in database stratification and channel weighting schemes, this work illustrates a path forward to improved GPROF estimation at both ends of the precipitation distribution in keeping with a physical, process-based approach toward better understanding of the global distribution of precipitation.

Great Lakes Convective Snow: a GPM passive microwave perspective.

4B-02
2:30pm
W120A

Lisa Milani (612)
Mark S. Kulie (MTU), Giulia Panegrossi (ISAC-CNR), Sarah E. Ringerud (NASA-GSFC 612), Jean-Franois Rysman (ISAC-CNR), Gail Skofronick-Jackson (NASA-HQ), Paolo Sanó (ISAC-CNR), Pierre E. Kirstetter (University of Oklahoma), Yalei You (UMD-ESSIC), Nai-Yu Wang (UMD-ESSIC)

Snowfall can be produced by different precipitating structures with distinctly different cloud macrophysical and microphysical compositions. Deep cloud structures related to synoptically-forced, large-scale systems, represent a common type of midlatitude weather events. Alternatively, many mid- to high-latitude oceanic and coastal regions are prone to shallow convective snow produced by cold air outbreaks interacting with unfrozen large bodies of water. The regional impact of the shallow convective snow cannot be ignored since

they often produce intense snowfall rates and influence regional hydrology. This work focuses on the ability of the Global Precipitation Measurement (GPM) passive microwave sensors of detecting and quantifying this particular snowfall mode over the US Great Lakes region. GPM's Microwave Imager (GMI) and constellation sensors brightness temperatures (TB) are used to detect any signal related to intense shallow convective snowfall events and the related Goddard PROfiling (GPROF) algorithm products are analyzed to understand strengths and weaknesses of the algorithm. In particular, the sensitivity of GPROF to some key parameters used to partition the GPROF a-priori database and converge more efficiently to the solution is investigated. These parameters are model-derived 2-meter temperature (T2m), total precipitable water (TPW), and background surface type. GPM's official GPROF frozen surface classification (different types of snow cover or sea ice) is compared to alternative classification schemes based on the low-frequency signal at the time of the radiometer overpass. The effective dependence of the GPROF snowfall rate estimates on the representativeness of shallow convective snowfall environmental conditions in the a-priori database is investigated. The Multi-Radar/Multi-Sensor (MRMS) quantitative precipitation estimates (QPE) database is used as ground reference for qualitative and statistical evaluations.

4B-03
2:45pm
W120A

Quantifying water storage change and land subsidence induced by the Bakun Dam, Malaysia, using multiple satellite data

Natthachet Tangdamrongsub (617)
Michael F. Jasinski (617)

The Bakun Dam, located in Sarawak Malaysia, is the largest hydropower dam in Southeast Asia. The dam commenced its operation in late 2010 causing a vast extent of the freshwater reservoir, changing the characteristic of Sarawak's rainforest and the natural flow of the regional river networks. The relocation of a significant amount of water storage not only affects the natural hydrological cycle but also leads to large-scale land subsidence over the area. This study, for the first time, will quantify the terrestrial water storage variation (TWS) and land subsidence induced by the Bakun Dam using multiple satellite observations (GRACE, Landsat), land surface models (CABLE, GLDAS, NCEP, ECMWF), and ground observations (GPS). During the 17-month impounding period, GRACE observes the increased TWS estimate of the Bakun Lake by approximately 200 mm and Landsat detects the increased lake extent by around 600 km2. The increased TWS and lake area estimates are corresponding to approximately 130 m surplus lake level derived by the forward models. The land surface models cannot capture the increased WS due to the incomplete water storage components used in the TWS simulation. The Bakun Dam induced surface displacement is determined using the disk load model associated with the GRACE-derived lake level and Landsat-derived lake extent. The commencement stage of the Bakun Dam induces the large-scale land subsidence, which causes the Earth's surface at the GPS-BIN1 station to subside by 10 mm, and moves toward the Bakun Lake by 5 mm. Incorporating GRACE with other remote sensing data allows the exploitation of the gravity signal at a much smaller spatial scale than its intrinsic resolution as demonstrated in this study.

Rainfall decline in West Africa forced by smoke and dust transport

4B-04
3:00pm
W120A

Amin Dezfuli (610.1)
Michael Bosilovich (610.1), Charles Ichoku (613)

Rainfall in West Africa during boreal summer is primarily controlled by the low-level southerly monsoon flow that transports moisture from the Gulf of Guinea to the region and the African Easterly Jet that modulates the convective systems. However, the role of aerosols in rainfall variability of this region, despite the large emissions of dust and black carbon in Africa, is not well-understood. Our study reveals a decline in precipitation over Southern West Africa (SWA) in the past two decades that its trend and interannual variability present an indirect relationship with the aerosols loadings. Examining the local and remote sources of aerosols, we found that the latter have a larger contribution. We have used MERRA-2 large scale atmospheric dynamics and physics data to determine the mechanisms responsible for aerosol-rainfall interactions in the region. Our results have important implications for the people and ecosystem as the increasing rates of land use change, deforestation and urbanization in the continent are expected to enhance the aerosols. This will result in an increase in the frequency and intensity of the extreme events including droughts.

Understanding the Water Cycle Above the North Polar Cap on Mars Using MRO CRISM Retrievals of Water Vapor

4B-05
3:15pm
W120A

Alain Khayat (693)
Michael D. Smith (693), Scott D. Guzewich (693)

The north polar cap (NPC) on Mars is the major reservoir of atmospheric water (H_2O) currently on Mars. The retrieval and monitoring of atmospheric water vapor abundance are crucial for tracking the cycle of water above the NPC. The Compact Reconnaissance Imaging Spectrometer for Mars (CRISM) aboard the Mars Reconnaissance Orbiter (MRO) has provided a wealth of data that extend over 5+ Martian years, covering the time period between 2006 and 2016. CRISM is ideally suited for spring and summer observations of the north polar region (latitudes poleward of 60°). The retrievals of water vapor column abundances over this extended period of time were performed over both ice-free and water ice covered surfaces, extending the coverage of the water vapor maps to include the permanent cap, where a maximum value of 90 precipitable micrometers (pr-μm) is retrieved, as compared to 60 pr-μm over ice-free regions in the North Polar Region. Away from summertime maximum, modest interannual variability in the water vapor abundance is observed. Zonal averages over all the observed Martian years combined show a developing water front that shifts northward towards summer, before dissipating over the permanent cap during mid-summer. A prominent feature at latitudes around 75° shows large abundances of water vapor, indicating a water vapor annulus encircling the retreating edge of the seasonal polar cap during late spring. Meridional transport of water modeled here show that the annulus may be a result of the convergence of water vapor from both south and north along the retreating edge of the NPC.

Session 4C: Exoplanets

Session chairs: Lauren Andrews & Greg Mosby

Analysis of OGLE-2017-BLG-0406Lb, a Planet Orbiting a Star Likely to be in the Galactic Bulge

4C-01
2:15pm
W120B

Yuki Hirao (667)
David Bennett (667), Clement Ranc (667), Aparna Bhattacharya (667)

Gravitational microlensing is an unique technique to detect exoplanets with sensitivity down to low mass beyond the snow line. This is because it is most sensitive to planets orbiting near the Einstein ring radius, which is a few AU from the host star, which makes it complementary to other methods. Detecting such planets is important for understanding the formation of systems like our solar system because gas and ice giant planets are believed to form beyond the snow line, where the protoplanetary disk is cold enough for ice to condense, in the core accretion theory. Microlensing is also sensitive to planets orbiting stars in the Galactic bulge, because microlensing events can be caused by stars at any distance between the Earth and the Galactic bulge, where most of the source stars reside. In the talk, we will present the analysis of planetary microlensing event OGLE-2017-BLG-0406. This event was observed both from ground and by Spitzer space telescope. Comparison of the light curves observed from the ground and by Spitzer allows us to constrain the distance to the planetary system using the microlensing parallax effect. We find the lens system consists of G or K type star orbited by a sub-Jupiter mass planet located at about 6.5 kpc away from the Earth, which is likely to be in the Galactic bulge. This event and others observed by Spitzer, will help us to measure the Galactic distribution of planetary systems.

Ongoing Variability in Transits of the Disintegrating Rocky Exoplanet K2-22b

4C-02
2:30pm
W120B

Knicole Colon (667)
TECH Collaboration

Of the thousands of exoplanets known, only three disintegrating planets have been identified to date around main-sequence stars. These disintegrating planets appear to have tails of dusty material that produce asymmetric transit shapes. K2-22b is one of these few disintegrating planets discovered to date, and its light curve not only displays highly variable transit depths but also uniquely displays evidence of a leading dust tail. Here, we present results from a large ground-based photometric observing campaign of the K2-22 system that took place between December 2016 and May 2017, which we use to investigate the evolution of the transit of K2-22b. Last observed in early 2015, in these new observations we recover the transit around the expected time and measure a typical depth of <1.5%. We find that the distribution of our measured transit depths is comparable to the range of depths measured

in observations from 2014 and 2015. These new observations also support ongoing variability in the K2-22b transit shape and time, although the overall shallowness of the transit makes a detailed analysis of these transit parameters difficult. We find no strong evidence of wavelength-dependent transit depths for epochs where we have simultaneous coverage at multiple wavelengths, although our stacked Las Cumbres Observatory data collected over days-to-months timescales are suggestive of a deeper transit at blue wavelengths. We encourage continued high-precision photometric and spectroscopic monitoring of this system in order to further constrain the evolution timescale and to aid comparative studies with the other few known disintegrating planets.

Advancing the Planetary Spectrum Generator to accurately characterize the diversity of exoplanetary atmospheres

4C-03
2:45pm
W120B

Vincent Kofman (693)
Geronimo L. Villanueva

The study of exoplanets is a relatively young and exciting field. New exoplanets are being discovered almost daily, and the diversity among them is stunning. To interpret the information from the range of atmospheres we can detect on these planets, new methods have to be developed. The Planetary Spectrum Generator (PSG) provides users with a full range of tools (geometric, spectroscopic as well as telescope characteristics) to simulate exoplanet spectra as would be seen by an observer. Spectra from high temperature atmospheres are computationally expensive to calculate, and require significant pre-processing. New methods are being incorporated in PSG to facilitate the simulation of high temperature exoplanet atmosphere spectra.

Nulling of an Actively-Controlled Segmented Aperture Telescope

4C-04
3:00pm
W120B

Brian Hicks (667)
Keith Jahoda (662), Padi Boyd (667), Michael McElwain (667), Neil Zimmerman (667), Sarah Logsdon (667), Maxime Rizzo (667), Pete Petrone (694), Matt Bolcar (551), Tyler Groff (551), Joe Howard (551), Alden Jurling (551), Ron Shiri (551)

We present current performance for the telescope, pointing, and coronagraph component subsystems of the Segmented Aperture Interferometric Nulling Testbed (SAINT). The project pairs an active segmented mirror with the Visible Nulling Coronagraph (VNC) towards enabling capabilities for the future space observatories needed to directly detect and characterize Earth-sized worlds around nearby stars. We describe approaches to optimize subsystem wavefront sensing and control parameters, summarizing relevant scaling relations between these parameters, residual errors, and observed contrast measurements. Preliminary results from diagnostic tests performed under various controlled conditions are discussed along with intermediate contrast measurements towards demonstrating the full system.

4C-05
3:15pm
W120B

Modelling exoplanet detection with the LUVOIR coronagraph

Roser Juanola-Parramon (660)

Neil T. Zimmerman (667), Maxime J. Rizzo (667), Giada N. Arney (693), Tyler Groff (551), Laurent Pueyo (STScI), Remi Soummer (STScI), Matthew Bolcar (551), Aki Roberge (667)

Direct imaging of exoplanets in their habitable zone is extremely challenging due to two main factors: the proximity of the planet to the parent star and the flux ratio between the planet and the parent star, usually to the order of 10^{-10} in the visible. Future missions like the Large UV-Optical-Infrared (LUVOIR) Surveyor and the Habitable exoplanet Imaging Mission (HabEx) require large apertures and coronagraphs with active wavefront control to be able to suppress the starlight so faint planets can be detected and characterized adjacent to their parent star. The Extreme Coronagraph for Living Planet Systems (ECLIPS) is the coronagraph instrument on the LUVOIR Surveyor mission concept. It is split into three channels: UV (200 to 400 nm), optical (400 nm to 850 nm), and NIR (850 nm to 2.0 microns), with each channel equipped with two deformable mirrors for wavefront control, a suite of coronagraph masks, a low-order/out-of-band wavefront sensor, and separate science imagers and spectrographs. The Apodized Pupil Lyot Coronagraph (APLC) is one of the baselined mask technologies to enable 10^{10} contrast observations in the habitable zones of nearby stars. The LUVOIR concept uses a large, segmented primary mirror (9-15 meters in diameter) to meet its scientific objectives. For such an observatory architecture, the coronagraph performance depends on active wavefront sensing and control and metrology subsystems to compensate for errors in segment alignment (piston and tip/tilt), secondary mirror alignment, and global low-order wavefront errors. Here we present the latest results of the simulation of these effects for different working angle regions and discuss the achieved contrast for exoplanet detection and characterization under these circumstances. Finally, we show simulated observations using high-fidelity spatial and spectral models of planetary systems generated with Haystacks, setting boundaries for the tolerance of such errors.

Poster Session

Session chairs: Lauren Andrews & Erwan Mazarico

Evaluation and validation of NASA's GMAO MERRA2 reanalysis surface winds

1P-01
3:30pm

David Carvalho (610.1)
Santha Akella (610.1)

MERRA-2 is the most recent reanalysis dataset produced and released by NASA's GMAO. Given the importance of an accurate and reliable representation of the global near-surface wind fields in contemporary reanalyses, the aims of this work are two-fold: i) to compare MERRA-2 surface winds with observations and also with its contemporary reanalyses (NCEP-CFSR, ERA-Interim and JRA55), in order to assess their accuracy, quality and to evaluate if they are in line with the other contemporary reanalyses surface winds; (ii), to assess the improvements in MERRA-2 representation of the global surface winds over its predecessor, MERRA. For that, 10 years of near-surface wind data from 5 reanalyses (MERRA-2, MERRA, ERA-Interim, NCEP-CFSR and JRA55) were compared with a wide variety of in-situ surface winds observations (land met stations, buoys, ships, space-borne scatterometers and microwave radiometers). Results show that the accuracy of MERRA2 surface winds is comparable to other modern reanalyses surface winds and also represent a clear improvement over its predecessor, MERRA, in terms of a realistic and reliable representation of the global near-surface wind fields. Moreover, all reanalyses showed lower errors in representing the wind fields over the tropics (with the exception of the Inter-Tropical Convergence Zone, ITCZ), while in higher latitudes the errors are higher, particularly near the poles.

What is the value of radiometer measurements in conjunction with multi-frequency radar data?

1P-04
3:30pm

Stephen (Joe) Munchak (612)
Ian Adams (612)

Radar and passive microwave radiometer are the pre-eminent tools used to remotely sense precipitation from space and aircraft, for mapping applications and process investigations. Owing to their separate heritage, differing viewing geometries and resolutions, and often the unavailability of both types of measurements simultaneously from the same platform, algorithms for the separate instruments have reached greater maturity than those that combine the passive and active measurements. In recent years, advancement in combined active-passive algorithms has been spurred by the Global Precipitation Measurement (GPM) mission, which derives precipitation profiles from Ku/Ka-band radar and multi-frequency radiometer measurements that are used in Bayesian retrievals across a constellation of passive

sensors, necessitating physical agreement between the active and passive measurements. This work will draw from the GPM combined algorithm as well as algorithms designed for use with airborne datasets to quantify the additional information provided by passive microwave radiometer measurements to multi-frequency radar in different regimes (e.g., land/ocean, convective/stratiform). The impact on retrieved integral and profile quantities as well as surface parameters will be presented. One particular quantity that benefits from the combination of slant-viewing radiometer and near-nadir radar measurements is a parameter that describes the bulk aspect ratio in the ice phase. With the next generation of cloud and precipitation observing satellites in the pre-formulation phase, suggestions for future instrument passive and active frequency combinations and viewing geometries will be given.

Using principal component analysis as a noise filter on Cloud Aerosol Transport System (CATS) daytime data

1P-05
3:30pm

Patrick Selmer (612)

Anthony Mamakos, John Yorks, Matthew McGill

Daytime data collected by the space-borne Cloud Aerosol Transport System (CATS) lidar are particularly noisy due to the solar background signal impinging on its photon counting detectors. CATS nighttime data does not have this issue. Substantial averaging of the daytime data is performed to achieve desirable SNR at the expense of information loss. Principle component analysis (PCA) offers a possible way to remove noise and limit averaging to retain higher resolution information of atmospheric features. Results of PCA applied to CATS data are shown and discussed.

A regional analysis of factors affecting the Antarctic boundary layer during the Concordiasi campaign and comparison with MERRA-2

1P-06
3:30pm

Manisha Ganeshan (613)

Yuekui Yang

This study explores the regional variability in factors affecting the atmospheric boundary layer over continental Antarctica using high-resolution dropsonde observations from the Concordiasi campaign in the austral spring of 2010. Analyses show that although the surface-based inversion (SBI) remains the dominant feature, well-mixed boundary layers, some with convective features, are observed with an occurrence frequency of 33% and 18% in West and East Antarctica, respectively. The boundary layer mixing is dominated by mechanical instability albeit with regional flavors caused by topographically forced winds, shortwave radiation, and air mass influences. In East Antarctica, the downsloping wind regime is prevalent, and related katabatic effects are strongest over high elevation slopes where the wind-induced turbulence is the primary cause of SBI erosion and boundary layer mixing. Previous studies over Dome C have demonstrated the significance of shortwave radiation for

mixed layer development during the peak of summer. While such an effect is not dominant during spring, solar forcing may contribute to turbulent mixing in high latitude regions. Well-mixed boundary layers are most frequently observed in the "moist tongue" region of West Antarctica, highlighting the importance of dynamical systems for boundary layer mixing. Additionally, we compare the stability representation in the Modern Era Retrospective analysis for Research and Applications version 2 (MERRA2), accounting for possible differences due to the coarser model vertical resolution compared to the high-resolution Concordiasi dropsondes. The impact of systematic errors in the model low-level temperature and wind fields and their contribution to the stability representation is investigated, following which recommendations are made for improving related parameterized processes in the NASA Goddard Earth Observing System (GEOS, version 5) model.

Impact of assimilating AIRS cloud-cleared radiances on the representation of Polar Lows

1P-07
3:30pm

Manisha Ganeshan (613)

Erica Mc-Grath Spangler (610.1), Oreste Reale (610.1), Will McCarty (610.1), Ron Gelaro (610.1)

Polar lows are mesoscale high-latitude cyclones that form over the ice-free ocean poleward of the midlatitude jet stream during winter and spring season. Due to their rapid growth at sub-synoptic scales in regions with very few traditional observations, prediction of polar lows using conventional assimilation methods remains challenging. This study explores the sensitivity of polar lows in the Southern Ocean to the assimilation of cloud-cleared AIRS (Atmospheric Infrared Sounder) radiances in the Goddard Earth Observing System (GEOS, version 5) data assimilation and forecast system during the austral spring 2014 season using observing system experiments (OSEs). Assimilating AIRS cloud-cleared radiances (CCR) instead of the current, operational clear-sky only radiances is found to benefit the representation of convectively-driven small-scale cyclones at high latitudes at no loss of global skill. In a manner previously noted for tropical cyclones, the assimilation of CCRs creates a temperature dipole over the top of meteorologically active and strongly convective systems such as Antarctic lows, which helps improve the analyzed representation of their scale and vertical structure.

1P-08
3:30pm

Investigating Air Pollution Gradients in the Chesapeake Bay with OWLETS

Natasha Dacic (614)

John T. Sullivan (614), Glenn M. Wolfe (614/JCEST), K. Emma Knowland (610.1/USRA), Timothy A. Berkoff (NASA Langley/475)

Influenced by multiple emission sources and complex meteorology, the Chesapeake Bay area continues to contribute to poor air quality for the surrounding urban regions. Measurements of pollution within difficult terrain and over bodies of water, such as the Chesapeake Bay watershed, have been historically problematic to obtain due to small-scale meteorological circulations. These difficulties pose challenges for air quality managers and scientists responsible for monitoring air quality. Air quality managers in coastal environments rely heavily on model simulations for understanding pollutants including surface level ozone (O_3). We present an ongoing investigation of the interaction between pollutants and coastlines from an intensive set of observations with the 2017 Ozone Water-Land Environmental Transition Study (OWLETS) campaign.

Measurements with airborne, shipborne, and ground-based instrumentation were taken mid-July to mid-August 2017 with an in-land site at NASA Langley Research Center (LaRC) and an over-water site at Chesapeake Bay Bridge Tunnel (CBBT). Vertical profile data from TOLNet lidars and ozonesondes in addition to remote sensing and in-situ observations of air quality were available from the campaign for analysis. Surface O_3 from NASA GMAO's GEOS composition forecast were modeled.

Two consecutive days of C-23 Sherpa flights showed elevated concentrations of O_3 and other greenhouse gases which prompted further investigation into the meteorological and model output data. Preliminary results showed that pollution gradients exist at the water-land transition region and air was transported from urbanized regions onto the water on July 20th. The TOLNet lidar analysis showed near continuous measured profiles of O_3 which highlight the concentration differences in-land versus over-water. The experimental surface O_3 model output shows elevated concentrations (80-100 ppbv) during the flight time for July 20th.

Continuation of OWLETS and the surface O_3 model output will increase understanding of the physical and chemical complexity of the water-land transition around the Chesapeake Bay, improve air quality management, and set the groundwork for future geostationary air quality instruments such as the NASA Tropospheric Emissions: Monitoring of Pollution (TEMPO).

Variations in Global Tropospheric OH Over the Last Several Decades

1P-09
3:30pm

Julie Nicely (614)

Timothy P. Canty (UMD), Michael Manyin (614/SSAI), Luke D. Oman (614), Ross J. Salawitch (UMD), Stephen D. Steenrod (614/USRA), Susan E. Strahan (614/USRA), Sarah A. Strode (614/USRA)

The oxidizing capacity of the troposphere is controlled primarily by the abundance of hydroxyl radical (OH). The global mean concentration of tropospheric OH, [OH]_TROP (the burden of OH in the global troposphere appropriate for calculating the lifetime of CH_4) inferred from measurements of methyl chloroform has remained relatively constant during the past several decades despite rising levels of CH_4 that should have led to a decline. Here we examine other factors that have affected [OH]_TROP such as the changing values of stratospheric ozone, rising tropospheric H_2O, varying burden of NOx (=NO+NO2), rising temperatures, and widening of the climatological tropics due to expansion of the Hadley cell. Our analysis suggests the positive trends in [OH]_TROP due to H_2O, NOx, overhead O_3, and tropical expansion are large enough (d[OH]_TROP = +0.95±.18% per decade) to counter almost all of the expected decrease in [OH]_TROP due to rising CH_4 (d[OH]_TROP = 1.01±.05% per decade) over the period 1980 to 2015, while variations in temperature contribute almost no trend (d[OH]_TROP = 0.02±.02% per decade) in [OH]_TROP. The approximated impact of Hadley cell expansion on [OH]_TROP is also a small, but not insignificant factor partially responsible for the steadiness of tropospheric oxidizing capacity over the past several decades, which free-running models likely do not capture.

Networked ground-based Pandora observations of enhanced tropospheric ozone associated with strong mid-latitude cyclones

1P-10
3:30pm

Joseph Robinson (614)

A. Kotsakis (614), R. Swap (614), G. Labow (614), T. Knepp (614), V. Connors (VCU), M. Tzortziou (614), A. Reynolds (W&M), J. Herman (614), J. Szykman (EPA)

Late winter and early spring is a period often associated with large numbers of extratropical disturbances in the northern mid-latitudes. Further, disturbances that develop into cyclones are critical to the balance of Earth's climate and are known to induce changes in atmospheric composition, including intrusion of stratospheric ozone into the troposphere. The late winter period of 2018 was an exceptionally explosive time for cyclogenesis in the eastern United States, with four northeasters, two achieving bomb status, developing in a period of three weeks from early to late March. During this time, as part of the NASA Pandora Project, a network of Pandora spectrometer systems was present throughout the eastern United States. In this study, we demonstrate the potential value of networked ground-based observations for tracking synoptic scale tropospheric ozone enhancement. To achieve this, networked Pandora observations were coupled with in-situ, remote sensing, and reanalysis datasets to provide a more complete picture of these events. We present Pandora and similar observations detailing enhanced total column as well as tropospheric ozone associated with

the passage of these storms and corroborate these observations with additional observational and reanalysis datasets. When coupled with the vertical resolution of reanalysis datasets and additional platforms, we argue a ground-based network of air quality/atmospheric composition observations are a valuable and economical tool for observing synoptic activity.

Evaluation of MERRA-2-based Ozone Profile Simulations with the Global Ozonesonde Network

1P-11
3:30pm

Ryan M. Stauffer (614)

Anne M. Thompson (610), Luke D. Oman (614), Susan E. Strahan (614)

Chemical transport model (CTM) hindcasts of ozone (O_3) are useful for filling in observational gaps and providing context for observed O_3 variability and trends. We use global networks of ozonesonde stations to evaluate the O_3 profiles in two simulations running versions of the NASA Global Modeling Initiative (GMI) chemical mechanism. Both simulations are tied to the NASA Modern-Era Retrospective analysis for Research and Applications, Version 2 (MERRA-2) meteorological reanalysis: 1) The GMI CTM, and 2) The MERRA-2 GMI Replay (M2 GMI). Both simulations start in 1980, and are compared against >50,000 ozonesonde profiles from 37 global stations from the tropics to the poles. The comparisons allow us to evaluate how the Replay technique affects modeled O_3 distribution, how an updated chemical mechanism in the GMI CTM affects simulated tropospheric O_3 amounts, and how observed O_3 distributions compare to the full set of model output. In general, M2 GMI O_3 is ∼10% higher than in the GMI CTM, and shows global near-surface and tropical upper troposphere/lower stratosphere (UT/LS) high biases. The updated chemical mechanism in the GMI CTM reduces these high biases. Both simulations show similar negative biases in tropical free-tropospheric O_3, especially during typical biomass burning seasons. The simulations are highly-correlated with ozonesonde measurements, particularly in the UT/LS ($r > 0.8$), showing the ability of MERRA-2 to capture tropopause height variations. Both simulations show improved correlations with ozonesonde data and smaller O_3 biases in recent years. We expect to use the sonde/model comparisons to diagnose causes of disagreement and to gauge the feasibility of calculating multidecadal O_3 trends from the model output.

The impact of boreal summer ENSO events on tropical lower stratospheric ozone

1P-12
3:30pm

Olga Tweedy (614)

Darryn W. Waugh (JHU), William J. Randel (NCAR), Marta Abalos (Universidad Complutense de Madrid), Luke D. Oman (614), Doug E. Kinnison (NCAR)

The interannual variability of Tropical Lower Stratosphere (TLS) ozone and its connections to sea surface temperatures (SSTs) in the equatorial Pacific are examined using a combination of chemistry climate model (CCM) simulations, satellite observations, and reanalyses. The model simulations and observations show large differences in the magnitude of interannual variability in ozone between Northern and Southern tropics (NT and ST respectively) during boreal summer, but small differences in winter. The interannual variability during boreal summer is highly correlated with summer SSTs in the eastern and central Pacific Ocean and El Niño Southern Oscillation (ENSO) events. Larger variability in NT ozone is primarily due to meridional advection, connected to the changes in the onset date and strength of the Asian Summer Monsoon (ASM) anticyclone. The ASM anticyclone forms earlier in a season and tends to be stronger during cold (La Nina) events leading to more isentropic transport of ozone from the extratropics into the NT, with the reverse for warm (El Nino) events.

Modeling the 21st century committed dynamical response of the Greenland Ice Sheet

1P-13
3:30pm

Isabel Nias (615)

Sophie Nowicki (615), Beata Csatho (University at Buffalo), Prashant Shekhar (University at Buffalo)

The Greenland Ice Sheet (GrIS) has been out-of-balance since the early 1990s, contributing to sea level at a rate of $\sim$0.4 mm/yr. This mass loss can be partitioned between surface (and basal) mass balance and discharge due to ice dynamics, predominantly through large outlet glaciers. While there is an instantaneous response in outlet glacier velocity to a perturbation at the terminus (e.g. a large calving event), the diffusive response due to the evolution of ice thickness over time means that the total effect of a perturbation can take decades to be fully realized. Here we model the committed sea level response of the GrIS. That is, overlooking any future perturbations or mitigation, we find the minimum sea level contribution from the GrIS over the coming decades, accounting for the slow dynamical response of the ice to past changes. We use the ice flow model ISSM, along with various input datasets, to find an initial state representing the ice sheet in the early 2000s, from which we run forward simulations, holding the climate constant. We apply perturbations to the outlet glacier termini that represent observed changes that occurred during the first decade of this century. Satellite observations of surface elevation change and gravimetry are used to determine how far the GrIS has deviated from this minimum response in recent years. The simulations that match well with contemporary changes are continued into the future, to give the committed sea level contribution from the GrIS over the 21st century.

Antarctic Ice Shelf Thickness Change from Multi-Mission Lidar Mapping

1P-14
3:30pm

Tyler Sutterley (615)
Thorsten Markus (615), Thomas Neumann (615)

We calculate rates of ice thickness change and bottom melt for ice shelves in West Antarctica and the Antarctic Peninsula from a combination of elevation measurements from Operation IceBridge corrected for oceanic and surface processes, surface velocity measurements from synthetic aperture radar, and high-resolution outputs from regional climate models. We calculate ice thickness change rates in a Lagrangian reference frame to reduce the effects from advection of sharp vertical features, such as cracks and crevasses, which can saturate Eulerian-derived estimates. We use our method over different ice shelves in Antarctica, which vary in terms of the processes that drive their change, their size and their repeat coverage but are all susceptible to short-term changes in ice thickness. We find that ice thickness variations of the Larsen-C ice shelf are due to the flux divergence of the shelf with firn and surface processes controlling short-term variability over our observation period. The Wilkins ice shelf is sensitive to short time-scale coastal and upper-ocean processes, and basal melt is the dominate contributor to the ice thickness change over the period. At Pine Island ice shelf in the critical region near in the grounding zone, we find that ice shelf thinning rates exceed 40 m/yr. The thickness change is dominated by strong submarine thinning. Regions near the grounding zones of the Dotson and Crosson ice shelves are thinning at rates greater than 40 m/yr, also due to intense basal melt.

Derivation of Ocean Inherent Optical Properties with Bayesian Neural Networks

1P-15
3:30pm

Erdem Karakoylu (616)
Susanne E. Craig (616)

For several decades, chlorophyll-a (Chl-a) and inherent optical properties (IOP), key metrics of marine ecological and biogeochemical processes, have been derived from ocean colour using empirical or semi-analytical methods with reasonable accuracy across a wide variety of water types. However, accurate retrieval of these parameters in optically complex waters, where atmospheric correction is challenging, remains elusive. We argue that it is time to modernize our approach to information retrieval from ocean colour in these challenging scenarios. Instead of trying to correct for the atmosphere by estimating and subtracting it, we propose to use signals that include the atmosphere as input to more sophisticated techniques. Among these techniques Bayesian Neural Networks (BNN) stand out. BNNs provide uncertainties out-of-the box for both neural net weights and predictions. By construction BNNs are highly regularized, making them resistant to over-fitting and thereby likely to perform well on unseen data. Moreover, BNN are built here with automatic feature relevance determination. These characteristics are crucial for drawing insights from model training, comparing and selecting models, and for producing informative predictions. We showcase the derivation of chlorophyll a and inherent optical properties using BNNs and

discuss the implication of the results in the context of existing missions, as well as NASA's upcoming PACE (Plankton, Aerosol, Cloud and Ocean Ecosystem) mission.

Irrigation Signals Detected from SMAP Soil Moisture Retrievals

1P-16
3:30pm

Patricia Lawston (617)
Joseph Santanello, Jr. (617), Sujay Kumar (617)

Irrigation can influence weather and climate, but the magnitude, timing, and spatial extent of irrigation are poorly represented in models, as are the resulting impacts of irrigation on the coupled land-atmosphere system. One way to improve irrigation representation in models is to assimilate soil moisture observations that reflect an irrigation signal to improve model states. Satellite remote sensing is a promising avenue for obtaining these needed observations on a routine basis, but to date, irrigation detection from passive microwave satellites has proven difficult. In this study, results show that the new enhanced soil moisture product from the Soil Moisture Active Passive satellite is able to capture irrigation signals over three semiarid regions in the western United States. This marks an advancement in Earth-observing satellite skill and the ability to monitor human impacts on the water cycle.

Insights on streamflow variability in the Lower Mekong River Basin using in-situ observations, modeling and NASA satellites

1P-17
3:30pm

Ibrahim Mohammed (617)
John Bolten (617), Raghavan Srinivasan, Venkat Lakshmi

The aim of this research is to advance the understanding of the streamflow variability of the Lower Mekong River Basin (LMRB) through the combination of modeling and satellite remote sensing. In this study, we utilized the Soil and Water Assessment Tool (SWAT) to examine the impacts associated with anticipated changes in the inflow from the Upper Mekong River. This work serves as a novel combination of remotely sensed satellite observations and a catchment scale model (SWAT). Two model sets were developed and assessed for this work. The first developed SWAT model enables the integration of satellite-based daily remote sensed precipitation (TRMM and GPM), air temperature (GLDAS), digital elevation model, soil information (HWSD), dam information layer, and land cover and land use data to drive SWAT model simulations over the Lower Mekong River Basin. The second SWAT model set developed was driven by in-situ climate observations as well as the above static layers. The SWAT models driven by remote sensing and in-situ climate data were calibrated and verified with observed runoff data at the watershed outlet as well as at multiple sites along the main stem of the Lower Mekong River. The SWAT model driven by remote sensing climate performed better in calibration and verification metrics as compared to the SWAT model driven by in-situ data. It is worth to mention here that the SWAT models' performance comparison was based on monthly flows output, so some amount of temporal and spatial aggregation may have masked individual event prediction or adds uncertainty.

The Mekong regional in-situ climate data network is sparse and over short temporal periods as compared to the available satellite remote sensing data. Therefore, we adopt the SWAT model driven by satellite remote sensing climate data. Our work results suggest that the Lower Mekong River streamflow is highly variable and has a low predictability (Colwell index of 32%). We find that release of more water from the upstream Mekong during rainy season would affect flood duration in terms of more flooded days and higher frequency of downstream occurrence of floods. Our results also suggest that releasing more water from upstream Mekong during rainy season (for instance by 30%) would imply a further reduction in the Lower Mekong streamflow predictability (i.e. Colwell index reduces to 25%). This means our ability to predict floods/droughts at the Lower Mekong River would be affected to if there are any anticipated changes (i.e. increase/decrease) from upstream flow releases. Results from this work present a framework for improving the decision-making process and aid to the Lower Mekong River Basin to address challenges in hydrologic modeling. The coupled model framework presented is part of SERVIR, a joint capacity building venture between NASA and the U.S. Agency for International Development, providing state-of-the-art, satellite-based earth monitoring, imaging and mapping data, geospatial information, predictive models, and science applications to improve environmental decision-making among multiple developing nations.

Systematic and Random Error Components in Satellite and Land Surface Model Soil Moisture Estimates

1P-18
3:30pm

Mahdi Navari (617)

Sujay V Kumar (617), Joseph A. Santanello (617), Christa D. Peters-Lidard (610), Michael Cosh (USDA)

The importance of soil moisture as a critical variable in the climate system is well established. Soil moisture regulates the water and energy exchange between the land surface and the overlying atmosphere. Therefore, realistic characterization of soil moisture helps to better understand the interaction of land surface and atmosphere. It is a long-established fact that the soil moisture estimates from different sources (i.e., in-situ, model, and satellite) show large discrepancies in both their temporal variability and long-term means. As a result, the global climatology of soil moisture is undetermined. Characterizing random error in soil moisture estimates has already been addressed in numerous studies. In particular, data assimilation approaches are often used to combine the information from models and satellite retrievals. These methods, however, only deal with the correction of the random errors components. Most data assimilation and intercomparison studies ignore the systematic error component in the soil moisture estimates, though such biases are often the source of important signals due to the significant heterogeneity and human modifications of the land surface. In this study, we use an error decomposition methodology to partition the errors in satellite retrievals and land surface model soil moisture estimates into systematic and random components. The results indicate that the systematic error in each of these soil moisture estimates is significantly higher than the random error component. At the domain-averaged scale, the systematic error component accounts for 88% and 63% of the total mean

squared error, for SMAP and SMOS retrievals. Similarly, across the LSMs, the contribution of the systematic error varies between 78% to 95%, averaged over the NLDAS2 domain. As a result, methods such as data assimilation focused on improving the random error component are likely to provide small improvements. The study also highlights the need for developing alternative methods for improving the inherent "bservability" and information content of soil moisture estimates.

The Value of Near Real-Time Flood Impact Information in a Disaster Response Scenario

1P-19
3:30pm

Perry Oddo (617)
John D. Bolten (617)

Information is a critical resource in disaster response scenarios. Data regarding the geographic extent, severity, and socioeconomic impacts of a disaster event can help guide emergency responders and relief operations, particularly when delivered in a timely manner. Earth science information from remote observations provides a valuable tool for assessing conditions – on the ground – more quickly and efficiently. Here, we demonstrate the value of a near real-time flood impact system in a disaster response scenario. MODIS imagery from NASA's Land, Atmosphere Near real-time Capability for EOS (LANCE) system is used to produce operational estimates of inundation depths and economic damages. These rapid Earth observations are coupled with a decision-analytical model to inform decisions on transportation routing and resource allocation. Our results illustrate how the application of near real-time Earth observations can improve the effectiveness and efficiency of disaster response operations.

NASA Unified Weather Research and Forecasting (NU-WRF) Model Simulations for the Brown Ocean Effect: A Case Study of Tropical Cyclone Kelvin

1P-20
3:30pm

Jinwoong Yoo (617)
Joseph A. Santanello (617), Sujay V. Kumar (617), Patricia M. Lawston (617), and J. Marshall Shepherd

A suite of numerical simulations of Tropical Cyclone Kelvin has been conducted using the NASA Unified Weather Research and Forecasting (NU-WRF) Model coupled with the NASA Land Information System (LIS) to understand the contributions of the latent heat fluxes (LHFs) from the land surface for the landfalling tropical cyclone to maintain or intensify its strength after its landfall. Since its development as a tropical low system over Tiwi Islands north of Darwin, Australia, the system travelled southwest along the northwestern coast of Australia, precipitating substantial amount of rain over the cluster of national parks in the northern part of the Western Australia. The system intensified into Category 1 Cyclone over the shallow Indian Ocean shore near Eighty Mile Beach on Feb 17, 2018. Cyclone Kelvin (2018) made its landfall in the evening on Feb 17, 2018 through the Eighty Mile

Beach while its strength increased to Category 2. The system survived over the desolate land with relatively barren soils until Feb 19, 2018 when it became a Tropical Low. Among the suite of eleven numerical simulations driven by three global datasets (i.e., ERA-Interim, GDAS (FNL), MERRA2), the NU-WRF coupled with the LIS model simulation driven by the GDAS data produced the closest results to observation in terms of its track and intensity. Model simulation analysis reveals that the Tropical Cyclone Maintenance or intensification (TCMI) was highly associated with the latent heat flux (more than 70 W s^{-1}) over the land surface precipitated by the system itself over the national park cluster region as well as about the center of the cyclone during the daytime.

Assessing the uncertainty in the terrestrial water budgets over High Mountain Asia

1P-21
3:30pm

Yeosang Yoon (617)

Sujay V. Kumar (617), Yonghwan Kwon, Barton Forman, Ben Zaitchik

We focus on assessing the errors and uncertainties in the key terrestrial water budget components of precipitation, evapotranspiration (ET), runoff, terrestrial water storage (TWS), snow depth/snow water equivalent, and snow cover over High Mountain Asia (HMA) using a suite of uncoupled land surface model (LSM) simulations. Precipitation is one of the most important forcing variables in LSM simulation. Thus, the ten gridded precipitation products spanning 1980 to 2017, including APHRODITE, CHIRPS, CMORPH , ECMWF, ERA-Interim/Land, GDAS, HAR, IMD, MERRA-2, and TRMM are evaluated first to assess which precipitation dataset tends to be more suitable for LSM simulations in HMA. To quantify the systematic and random error in these precipitation datasets, inter-comparison with each other and a triple collocation analysis are applied. The consistency of their long-term trends is also evaluated. The Mann-Kendall, a nonparametric test is used for the trend analysis. Then an ensemble of LSM simulations with the selected precipitation dataset that provides the most consistent representation is performed to produce the terrestrial water budget estimates and their uncertainties. In this study, three different land surface models (i.e., Noah 3.3, Noah-MP 3.6, and Catchment F2.5) in the NASA Land Information System are employed. To evaluate the uncertainties in water budget estimates, reference measurements from remote sensing and reanalysis products (e.g., ALEXI and GLEAM for ET, GRACE for TWS, and MODIS snow products for snow cover) are used. Together, these evaluations provide a consistent assessment of the uncertainties in the water balance over HMA, bounded by available observations.

An observational study on CME flux ropes near the Sun

1P-22
3:30pm

Sindhuja Gunaseelan (671)
Nat Gopalswamy (671)

Our aim is to study Coronal Mass Ejection (CME) flux ropes and their source magnetic properties at the Sun. For this, we make use of the FRED (Flux Rope from Eruption data) technique that combines the source magnetic properties and the fluxrope geometric properties to fully describe the 'magnetized' flux ropes in terms of the axial field strength and the poloidal and toroidal fluxes. We consider 22 eruptive events, that show core and secondary dimmings and clear post eruption arcades (PEAs). The core and secondary dimmings are related to the toroidal and poloidal fluxes of the flux rope formed due to the reconnection process in the eruption region (Dissauer et al 2018). We obtained the poloidal flux by computing the reconnected (RC) flux from source regions using the PEA technique recently developed by Gopalswamy et al. (2017). Secondary dimming and RC flux have a positive correlation of 0.59 with 95% confidence intervals (0.22,0.85). The Core dimming and RC flux also show a positive correlation of 0.57 with 95% confidence intervals (0.19,0.79), we also found a relation between the two, which is Core =0.250.71 RC . We found that the poloidal flux is much greater than the toroidal flux as is expected from theoretical considerations for force free flux ropes. These results will help in realistic characterization of CME initiation needed for forecasting the geoeffectiveness of CMEs.

Kinematics of Earth directed CMEs associated with Type IIs using STEREO observation

1P-23
3:30pm

Suresh Karuupiah (671)
N. Gopalswamy (671)

Coronal Mass Ejections (CMEs) are huge expulsion of mass from the Sun into the interplanetary medium. CMEs originating from the disk center of the Sun are subject to projection effects. For such events, the true speed cannot be measured from coronagraphic images. So, we select halo CMEs in SOHO field of view such that they are observed in quadrature by one of the STEREO spacecraft (STEREO A or B). These halo CMEs in SOHO view appear as limb CMEs in STEREO view. The kinematic properties of such CMEs can be measured without projection effects. We select 26 halo CMEs to compare their kinematics with the properties of the associated interplanetary radio bursts. In particular, we compare the white-light shock properties with the frequency extent of the type II bursts. We use the graduated cylindrical shell (GCS) model to fit flux rope to the CME and obtain the shock standoff distance from which we can derive the shock Mach number. We use the Mach numbers to analyze the type II producing capability of the 26 CMEs.

Does the Magnetic Expansion Factor play a role in Solar Wind Acceleration?

1P-24
3:30pm

Samantha Wallace (671)
Charles N. Arge (671)

For the past 25+ years, the magnetic expansion factor (fs) has been a parameter used in the calculation of terminal solar wind speed (vsw) in the Wang-Sheeley-Arge (WSA) coronal and solar wind model. The magnetic expansion factor measures the rate of flux tube expansion in cross section between the photosphere out to 2.5 solar radii (i.e., source surface), and is inversely related to vsw (Wang & Sheeley, 1990). Since the discovery of this inverse relationship, the physical role that fs plays in solar wind acceleration has been debated. In this study, we investigate whether fs plays a causal role in determining terminal solar wind speed or merely serves as proxy. To do so, we identify pseudostreamers, which occur when coronal holes of the same polarity are near enough to one another to limit field line expansion. Pseudostreamers are of particular interest because despite having low fs, spacecraft observations show that solar wind emerging from these regions have slow to intermediate speeds of 350-550 km/s (Wang et al., 2012). In this work, we develop a methodology to identify pseudostreamers that are magnetically connected to spacecraft (i.e., ACE, STEREO-A & B) using WSA output derived with synchronic ADAPT input maps. We utilize this methodology to track the parcel of solar wind that left the pseudostreamer and obtain the spacecraft-observed solar wind speed for those field lines. We then compare the magnetic expansion factor of the last open field line on either side of each pseudostreamer cusp with the observed solar wind speed from spacecraft magnetically connected to the region. We identified 37 pseudostreamers and performed a statistical analysis to determine the correlation of fs at pseudostreamer cusps and the terminal speed of the emerging solar wind. Our results show that there appears to be no correlation between fs and vsw at pseudostreamer cusps. Future work will involve looking at the compositional signatures of the solar wind for each pseudostreamer, and will explore the role of fs in modulating the fast solar wind along continuously open field lines using Ulysses observations deep inside coronal holes.

Formation and Magnetospheric Impacts of the Foreshock Bubble

1P-25
3:30pm

Sun Hee Lee (674)
David Sibeck (674), Marcos Vinicius (674)

We present multi-point observations of foreshock transient events and their impact on the Earth's magnetosphere. The four Magnetospheric Multiscale (MMS) spacecraft observed two discontinuities in a quasi-perpendicular bow shock regime on 18 December 2017. A textbook example of a foreshock bubble (FB) was observed in the region upstream of the first discontinuity. The FB is identified by a greatly decelerated and deflected antisunward flow, a significant increase in temperature, and depressed plasma densities and magnetic field strengths in the core of the FB. There is only one shock and it lies on the upstream side of the discontinuity. No bubble attends the second solar wind discontinuity. We will

investigate the relationship between the formation of the foreshock bubble and the IMF/solar wind conditions and the local/global impacts of each discontinuity with/without a foreshock bubble on Earth's magnetosphere and ionosphere. We note the presence of enhanced fluxes of energetic particles (E > 50 keV) within both the FB event and the second discontinuity and will address the sources and acceleration mechanisms for these energetic particles.

Simulated Parker Solar Probe Encounters with Dynamic Structures in the Slow Solar Wind

1P-26
3:30pm

Merrill Roberts (674)

A. K. Higginson (JHU-APL), B. J. Lynch (UC-Berkeley Space Sciences Laboratory), C. R. DeVore (674), V. M. Uritsky (CUA/671), J. T. Karpen (674), S. K. Antiochos (670)

The slow solar wind is observed both near the heliospheric current sheet (HCS) and at high heliospheric latitudes. Its composition suggests that the slow-wind plasma originates in the hot, closed-field corona, but migrates into the open-field corona where it can flow away freely into the heliosphere. The Separatrix-Web theory gives a compelling explanation of how the characteristics of the slow solar wind result from dynamics at the coronal open/closed boundary (Antiochos et al. 2011). Numerical simulations of S-Web dynamics have demonstrated that simple driving at the solar surface produces ubiquitous interchange reconnection all along the open/closed boundary, which maps to the HCS and S-Web arcs (Higginson et al. 2017a,b). Further analysis of those simulations has revealed the persistent formation and propagation of twisted flux ropes and torsional Alfven waves along the HCS and S-Web arcs (Higginson & Lynch 2018). The Parker Solar Probe (PSP) mission now has the opportunity to sample these slow wind regions in situ and to quantify their structure and dynamics. Signatures expected during encounters between PSP and coronal-hole jets have already been derived from our simulation data for interchange-reconnection-driven null-point topologies (Roberts et al. 2018). We here use the data-extraction and PSP-trajectory techniques developed for our investigation of jets to analyze the S-Web dynamic structures over the range of heliospheric radii to be traversed by PSP. The methods enable us to account simultaneously for the propagation of disturbances out into the heliosphere with the wind and the orbital motion of the spacecraft about the Sun. We here present preliminary results from this study, including the in situ plasma and magnetic-field signatures derived from the S-Web simulations and discuss the prospects for identifying them in the PSP data.

Validation of TIMED/SABER v2.0 operational temperature data with ground-based lidars between 75-105 km altitude.

1P-27
3:30pm

Erin Dawkins (675)

A Feofilov, L Rezac, AA Kutepov (675/CUA), D Janches (675), J Hffner, X Chu, X Lu, MG Mlynczak, J Russell III

The NASA Thermosphere Ionosphere Mesosphere Energetics and Dynamics (TIMED) Sounding of the Atmosphere using Broadband Radiometry (SABER) instrument performs near-global measurements of the vertical kinetic temperature (T_k) profiles and volume mixing ratios of various trace species (including O_3, CO_2, and H_2O), with data available from 2002 to present. Here we present the first comparative study of the latest publicly available SABER v2.0 operational T_k dataset relative to high-resolution ground-based lidar profiles. Collocated multiyear seasonally averaged-T_k-profiles were compared at nine different locations, representing a range of different latitudes. In general, the SABER v2.0 and lidar mean seasonal-T_k-profiles agree well, with the smallest absolute values of $\Delta T_k(z)$ (SABER minus lidar) found between 85 and 95 km, where the respective SABER and lidar uncertainties were smallest. At altitudes $\geq$100 km, the SABER $T_k(z)$ typically exhibited warmer temperatures relative to lidar, whereas the reverse was true for altitudes $\leq$85 km where SABER $T_k(z)$ was cooler. Overall, SABER was able to reproduce the general latitude- and season-specific variations in the lidar-T_k-profiles and shown to be statistically similar for most seasons, at most locations, for the majority of altitudes, and with no overall bias.

Modeling Geomagnetic Variations using a Machine Learning Framework

1P-28
3:30pm

Burcu Kosar (675)

Chun Ming Mark Cheung, Bala Poduval, Casey Handmer, George Gerules, Graham Mackintosh, Andres Munoz-Jaramillo, Monica Bobra, Troy Hernandez, Ryan Michael McGranaghan

We present a framework for data-driven modeling of Heliophysics time series data. The Solar Terrestrial Interaction Neural net Generator (STING) is an open source python module built on top of state-of-the-art statistical learning frameworks (traditional machine learning methods as well as deep learning). To showcase the capability of STING, we deploy it for the problem of predicting the temporal variation of geomagnetic fields. The data used includes solar wind measurements from the OMNI database and geomagnetic field data taken by magnetometers at US Geological Survey observatories. We examine the predictive capability of different machine learning techniques (recurrent neural networks, support vector machines) for a range of forecasting times (minutes to 12 hours). STING is designed to be extensible to other types of data. We show how STING can be used on large sets of data from different sensors/observatories and adapted to tackle other problems in Heliophysics.

Plasma Dynamics Associated With Equatorial Ionospheric Irregularities

1P-29
3:30pm

Jonathon Smith (675)

The Communication/Navigation Outage Forecasting System satellite was operational from 2008, a period of deep solar minimum, to 2015, a period of moderate solar conditions. The behavior of the vertical plasma drift and the distribution of plasma depletions during the deep solar minimum of 2009 deviated substantially from the behavior that was observed during the solar moderate conditions encountered by the Communication/Navigation Outage Forecasting System satellite in 2014, which are typical of previous observations. Presented here are observations of the vertical drift of plasma depletions and the background plasma in which they are embedded. We find that depletions detected at local times after 2100 hr during solar minimum are typically found in background drifts that are weakly downward compared to the strongly downward background drifts observed during moderate solar activity levels. Additionally, at solar minimum, the drift within the depletions is upward with respect to the background as compared with observations at the same local times during solar moderate conditions for which the depleted plasma more nearly drifts with the background. We note that weak background plasma drifts observed throughout the night during solar minimum promote the continued growth of depletions that may evolve more slowly or be continuously generated to appear in the topside in the postmidnight hours.

An Infrared Survey of Volatiles in Comet 252P/LINEAR Following a Close Approach to Earth

1P-30
3:30pm

Maria Camarca (690)

Lucas Paganini (693), Geronimo Villanueva (693), Sara Faggi (690), Manuela Lippi (690), Michael Mumma (690)

Cometary nuclei are considered primordial leftovers from the nativity of our solar system. The composition of their native ices encodes traces of the chemical and physical conditions that occurred during the formation of the early solar system – some 4.6 Gyr ago. Comets reside in two dynamical reservoirs: the Oort Cloud and the Kuiper Belt, allowing such information to be preserved throughout the years. Gravitational effects, however, can perturb cometary trajectories, throwing them toward the inner solar system. As these bodies approach the inner solar system, solar radiation triggers the sublimation of volatiles, releasing gas and dust from the icy nuclei that contain the information stored 4.6 Gyr ago. We can study this chemical composition remotely using ground-based infrared telescopes. Among others, a robust catalog of these cometary volatiles is essential to: 1) illuminate what chemistries abounded in the young solar system and 2) probe the role comets played in delivering the young Earth its oceans and organics. In this poster, we present preliminary results of Comet 252P/LINEAR using the Keck telescope in Hawaii, a rare object that had a historically close approach to Earth in March 2016. We will place 252P's molecular profile in context of other Jupiter Family Comets and the Oort Cloud Comet population using our Keck observations in April 2016.

1P-31
3:30pm

New emerging chemical taxonomy of comets observed in the IR between 1999 and 2016

Manuela Lippi (690)

Geronimo L. Villanueva (693), Michael J. Mumma (690), Sara Faggi (690)

Comets are cryogenically preserved relics from the early solar system. Cometary compositional properties (molecular abundances, isotopic ratios, spin temperatures) are directly relevant to understanding the processes affecting material in protoplanetary system formation and the origins of our planetary system. Since molecular abundances in comets are strongly influenced by temperatures, available atomic abundances and impinging radiation at the time of formation, the study of cometary nuclei composition could help in decoding the cosmogonic indicators that can reveal information about the prevailing physical and chemical conditions in the early Solar System, 4.6 billions of years ago; moreover they could test the hypothesis that small icy bodies have delivered prebiotic matter to early Earth. In the last 20 years cometary nuclei has been observed, mostly through ground-based observations, targeting the 3 - 5 μm infrared spectral region and using different high resolution spectrometers (NIRSPEC, CSHELL, CRIRES). In this region it is possible to observe and quantify primary molecules, released directly from the nucleus, as for example H_2O, CO, CH_4, CH_3OH, C_2H_6, C_2H_2, HCN, NH_3, H_2CO. So far, our archive collects data relative to 60 comets. Despite the small number of observed comets, the amount of data for each target is particularly large, making this the most rich and extensive database on comets realized till now. During this time we have greatly improved our ability to observe and analyze cometary spectral features, building more and more advanced data processing routines and realistic fluorencence quantum band models (Bonev 2005, Lippi et al 2013, Villanueva et al 2011, Villanueva et al 2012a and 2012b) that comprise a full line list for a specific vibrational band, use updated energy tables and correct for the solar field (Swings effect). In addition we improved the atmospheric model, introducing the Planetary and Universal Model of Atmospheric Scattering (PUMAS - Villanueva, G. L. et al (2015)), that integrates the latest radiative-transfer methods and spectroscopic parameterizations via line-by-line calculations. Considering that data analysis techniques and molecular models have been continuously changed and improved in these years, it emerges that the comparisons between the chemical composition of different comets may be affected by different reduction and retrieval approaches. We recently developed automated schemes that allow us to process our extensive cometary database in a systematic and accurate manner, giving us the opportunity to re-analyze the cometary spectra in a consistent manner, so to provide the most accurate database of molecular abundances and related parameters. Using a robust and common set of analytical tools we can now correct for data reduction related unevenness; by extracting abundance ratios, spin temperatures and deuterated fractions we can finally investigate their interrelationships and their true cosmogonic significance. We present the new molecular abundances, rotational temperatures and mixing ratios that we obtained using our new methodology applied to 10 comets selected from our archive. These comets were observed with the Near Infrared Echelle Spectrometer (NIRSPEC) at W. M. Keck Observatory located on Mauna Kea, Hawaii, from 1999 to 2016. We observe significant improvements in the confidence limits and some differences in the retrieved values, especially for comets observed before the advent of the new developed atmospheric and quantum models. Moreover, we were able to complete the old results with

primary and secondary molecules that were not identified and/or studied in the past due to the lack of molecular models (for example NH_3, NH_2, CN). The improvements in data reduction have given us the opportunity to observe new emission lines that could be related to molecules expected in comets but not yet observed and/or studied (for example C3H8 or C2H5D). Once the data relative to all the comets from the archive will be reduced and analyzed, we plan to use data mining (or similar) techniques that will help us to find possible new correlations and trends among different objects, and to build a new reliable taxonomy for comets.

Complex cyanides, cosmic rays, and chemical segregation in high-mass star-forming region G35.20+0.74N

1P-32
3:30pm

Veronica Allen (691)

In the study of high-mass star formation, hot cores are empirically defined stages where chemically rich emission is detected toward a high-mass protostar. It is unknown whether the physical origin of this emission is a disk, inner envelope, or outflow cavity wall and whether the hot core stage is common to all massive stars. With the advent of the highly sensitive sub-millimeter interferometer, ALMA, the ability to chemically characterize high mass star forming regions other than Orion has become possible. These sensitive high resolution observations have opened up opportunities to find small scale variations in young protostellar sources. Taking a two part approach, we investigate the chemistry of the hot cores within star-forming region G35.20-0.74N (G35.20) using high spatial resolution ($\sim$1000 AU) Cycle 0 ALMA observations and rate-equation-based chemical models. The observational analysis uncovered an interesting asymmetry in the distribution of the Nitrogen-bearing species (especially those with the CN-group) within G35.20 B. This was unexpected as this source contains a candidate Keplerian disk and such a segregation in chemistry is unexpected because of the short dynamical time-scale of the system. My poster will outline the observational result and results of our follow-up chemical modelling to determine a cause for small scale chemical segregation, and therefore the usefulness of complex cyanides as chemical clocks.

1P-33
3:30pm

Laboratory Studies of the Radiolytic Destruction of Biological Nucleobases in Icy Planetary Environments

Christopher K. Materese (691)

Perry A. Gerakines (691), Marla H. Moore (691), Reggie L. Hudson (691)

Icy worlds such as Europa and Enceladus have the potential to support life in their subsurface oceans. Initial evidence of the existence of such life may come in the form of biomarkers detected near the surfaces of these bodies. Efforts to detect such biomarkers are complicated by radiation induced chemistry that drives the modification and destruction of these compounds. Studying the radiolytic destruction of potential biomarkers and their dose dependent decay rates is important for future mission planning and for making sense of the data returned from such missions. In support of this objective, the Cosmic Ice lab has begun studying the radiolytic destruction of the five biological nucleobases adenine, guanine, cytosine, uracil, and thymine. Using a Van de Graaff accelerator, we subject micrometer-thin films of these compounds and diluted mixtures of these compounds in H_2O and CO_2 at low temperatures (< 150 K) containing these nucleobases to MeV protons and monitoring their destruction using infrared spectroscopy. Decay rate constants have been determined under a range of temperatures and ice compositions. Preliminary results and implications of this work for future missions will be presented.

1P-34
3:30pm

Amino Acids in Antarctic Micrometeorites

Eric Parker (691)

Cecile Engrand (CSNSM, CNRS/Univ. Paris Sud, Universit Paris-Saclay, France), Jason P. Dworkin (691), Daniel P. Glavin (690)

Delivery of organics by asteroids, comets, and their fragments may have contributed to the origin of life on Earth and possibly elsewhere. Carbonaceous chondrite studies suggest amino acids are present on asteroids and comets. The abundances, distributions, and isotopic and enantiomeric compositions of amino acids are vital for indicating processes and chemical compositions of parent bodies.

Compared to meteoritic organics, far less is known about organics in cosmic dust grains, including micrometeorites (MMs). MMs are the dominant source of extraterrestrial material accreted by Earth, contributing $\sim 30 \times 10^6$ kg/yr. MMs in the 100 - 250 μm size range deliver $\sim$1000$\times$ more mass than other exogenous debris.

The non-protein amino acid α-aminoisobutyric acid (α-AIB) was reported in batches of large (100 - 400 μm) Antarctic MMs (AMMs) from Cap Prud'homme, Antarctica and the South Pole Water Well. However, it remains unclear if MMs contain a broad distribution of amino acids that can serve as indicators for parent body processes.

Here, we report the analysis of six AMM grains ($\sim$7 μg total mass). Samples were analyzed by ultraperformance liquid chromatography with fluorescence detection and time-of-flight mass spectrometry, following pre-column derivatization with *o*-pthaldialdehyde/N-acetyl-L-cysteine, a chiral tagging agent that enhances analytical specificity for primary amines and provides enantiomeric separation of primary amino groups with chiral centers.

Non-terrestrially contaminated amino acids were detected in our analysis, which used ∼1000× less material than previous MM studies. We observed an amino acid distribution with elevated abundances of straight-chained n-ω-amino acids. Such a distribution was previously observed in thermally altered CV3 and CO3 chondrites, but not prominent in low temperature, aqueously altered CI, CM, and CR chondrites. Atmospheric entry heating may have influenced the amino acid distribution observed here, which warrants further exploration.

These findings demonstrate, for the first time, that amino acid distributions in cosmic dust can be used as an indicator for parent body processes and that MMs could have delivered a more diverse set of amino acids to the early Earth than previously thought (i.e., previously, only α-AIB was thought to be of extraterrestrial origin in MMs).

Alcohols in Carbonaceous Chondrites: Method Development for Investigating Chirality and Stable Isotopic Compositions

1P-35
3:30pm

Danielle Simkus (691)

D. N. Simkus (691), J. C. Aponte (691), J. E. Elsila (691), J. P. Dworkin (691)

The organic contents of carbonaceous chondrite meteorites provide a chemical record of the prebiotic synthesis reactions that took place during early solar system formation and during asteroidal alteration. These reactions, yielding a wide range of prebiotic organic compounds (e.g. amino acids, carboxylic acids, amines, aldehydes and ketones), may have played a key role during the origins of life and homochirality on Earth. Nevertheless, the formation relationships between the different meteoritic compound classes are not fully understood. In particular, the origin and distribution of meteoritic alcohols remain a significant gap in the literature as neither their stable isotopic ratios ($d_{13}C$) nor their enantiomeric compositions have been measured to date. Alcohols can be oxidized to produce aldehydes and ketones, which may be converted to amino acids via Strecker synthesis. Therefore, the presence or absence of enantiomeric excesses for chiral alcohols will shed light on the origin of L-enantiomeric excesses observed for some meteoritic amino acids. Additionally, comparing the alcohol d13C compositions to those of other meteoritic organic compounds will provide valuable insight into the roles of specific synthetic relationships. We present the early results from developing a method to simultaneously investigate the chirality and stable isotopic compositions of alcohols in meteorites.

Modeling the Neon Distribution measured by LACE in the Lunar Exosphere

1P-36
3:30pm

Orenthal Tucker (695)

Rosemary M. Killen (695), David R. Williams (690), Jaekyun Park, Sang-Joon Kim

During the Apollo 17 mission the Lunar Atmospheric Composition Experiment (LACE) instrument measured the variation of neon in the exosphere during the lunar night at Taurus-Littrow Valley (TLV) (20 N, 30 E). This data was recently analyzed for the first time in Killen et al. (2018, submitted to Icarus). The measurements indicate an event occurred during the 3rd and the 4th lunations that significantly altered the time dependence of the exospheric densities at TLV. On March 13, 1973 just before the night (on nearside) of the 3rd lunation, a teleseismic event was measured by the seismometers of the Apollo Passive Seismic Net. The event occurred at 84 S, 134 W (epicenter), and it was one of largest to have ever been recorded (Nakamura, 1979, Proc. Lunar Planet. Sci. Conf. 10th, 2290). We present results obtained from a Monte Carlo simulation of the 1973 seismic event for comparison to the LACE measurements to further our understanding of the complex relationship between source and loss processes of the lunar exosphere.

Age Distribution of Lunar Impact-Melt Rocks in Apollo Drive-Tube 68001/2

1P-37
3:30pm

Natalie Curran (698)

B. A. Cohen (698), B. Frasl (698), D. M. Bower (699)

Understanding the bombardment history of the Earth-Moon system is a key scientific goal of the planetary science community for determining the modification of the lunar crust, as well as understanding the evolution of the inner Solar System. Determining the ages and compositions of impact-melt rocks, in returned sample collections (Apollo and Luna) and lunar meteorites, have been used to address questions related to the impact history in the Earth-Moon system in addition to investigating the regional geology at collection sites. However, older impact-melt rocks may be gardened back into the regolith column, potentially making them volumetrically rare at the surface. Whereas, the opposite may be true for the youngest impact-melt rocks which could be oversampled nearest the surface, particularly those collected near small, young craters. Therefore, the role of gardening could have caused a possible bias affecting the preservation of impact-melt samples in the near-surface regolith and needs further clarification. Choosing samples from various depths in the lunar regolith is one way to understand the changes in impact-melt sample population that have been affected by gardening. The Apollo 16 double-drive tube 68001/68002 provides the opportunity to evaluate variations in age and composition of impact materials with depth. Previous work has determined five compositionally distinct units in the core based on composition and the soil maturity parameter Is/FeO. A small inflection in the Is/FeO profile at 3 cm depth in the core, may be related to the nearby South Ray impact event. As the five horizons can be distinguished from each other, each may contain a potentially distinct population of impact-melt rocks. These distinctions can provide an understanding of the complex history at the

Apollo 16 site, as well as shed light on the gardening effect on these populations of samples. We have chosen 50-70 particles from six bulk soils at various depths in 68001/2. These particles have been mounted, polished and analyzed for their texture and mineral chemistry. Based on these data, eleven textural groups were determined and representative particles will be chosen from each group to conduct trace-element analysis, followed by Ar-Ar dating techniques.

Analyses of Crystalline and X-ray Amorphous Materials in Gale Crater Rocks and Soils

1P-39
3:30pm

Cherie Achilles (699)

R. T. Downs (Univ. of Arizona), D. W. Ming (JSC), E. B. Rampe (JSC), R. V. Morris (JSC), A. C. McAdam (699), CheMin Science Team

The Mars Science Laboratory (MSL) rover, Curiosity, is exploring the layered sediments of Gale crater with the primary goal of finding and assessing environments that are, or once were, favorable habitats for life. Curiosity's scientific payload was designed to analyze the mineralogical, geochemical, and textural properties of rocks and soils encountered by the rover. Among this payload is the CheMin X-ray diffractometer, an instrument that provides data to determine the distribution of crystalline, clay mineral, and amorphous phases in each analyzed sample. Here, we present the mineralogy and amorphous chemistry of eolian deposits and mudstones from Gale crater and discuss how these data are important to understanding sediment sources, weathering histories, depositional environments, and diagenetic processes that influenced the formation of analyzed soils and rocks.

Impact of clouds and hazes in the JWST simulated transmission spectra of TRAPPIST-1 planets in the habitable zone

1P-40
3:30pm

Thomas Fauchez (699)

M. Turbet, A. Mandell, R. Kopparapu, G. Arney, E. T. Wolf, S. D. Domagal-Goldman, G. Villanueva, G. Suissa

M-dwarfs are the most common type of stars in our galaxy. Ultra-cool dwarfs (T $<$ 2700 K) are a sub-stellar class of late M-dwarfs and represent nearly 20% of astronomical objects in the stellar neighborhood of the Sun. Their smaller size than regular M-dwarfs allows easier detection of rocky exoplanets in close orbits, and this potential was recently realized by the discovery of the TRAPPIST-1 system. Located about 12 pc away, TRAPPIST-1 has seven known planets, and it is one of the most promising rocky-planet systems for follow-up observations due to the depths of the transit signals. Transit-timing variation (TTVs) measurements of the TRAPPIST-1 planets suggest terrestrial or volatile-rich composition. Also, it has been found that three planets (TRAPPIST-1 e, f and g) are in the Habitable Zone (HZ) where surface temperatures would allow surface water to exist. These planets will be prime targets for atmospheric characterization with JWST owing to their relative proximity to Earth and frequent planetary transits. Atmospheric properties are major components of

planet habitability. However, the detectability of gaseous features on rocky planets in the HZ may be severely impacted by the presence of clouds and/or hazes in their atmosphere. We have already seen this phenomenon in the "flat" transit transmission spectra of larger exoplanets such as GJ 1214b, WASP-31b, WASP-12b and HATP-12b. In this work, we use the LMDG global climate model to simulate several possible atmospheres for TRAPPIST-1 e, f and g: 1) Archean Earth, 2) modern Earth and 3) CO_2-dominated atmospheres. We coupled the GCM outputs with a 1D photochemical model (atmos) at the terminator to model photochemical hazes (especially for the Archean Earth-like atmospheres). We also calculate synthetic transit spectra using the GSFC Planetary Spectrum Generator (PSG), and we determine the number of transits needed to observe key spectral features for both JWST NIRspec and MIRI instruments. We have explored differences in transit depth (and altitude) between cloudy/hazy and clear sky spectra and between equilibrium chemistry and photochemistry assumptions, and calculated the number of transits needed to detect individual spectral features. Preliminary simulations have found that the planets with the most habitable conditions (TRAPPIST-1e with large ice-free oceans) also produce the highest fraction of cloud coverage, which then totally (or partly) hide biosignature gases (CH_4, O_2, O_3) and water vapor detection through transmission spectroscopy with JWST. Further results on the impact of photochemistry and prospects for observational constraints on atmospheric composition and ocean coverage will also be presented.

1P-41
3:30pm

Ab initio study of chromium isotpes

Der-you Kao (699)

Shawn Domagal-Goldman (693)

Isotope fractionation in chromium (Cr) isotope system, a recently emerging atmospheric O_2 proxy, has the potential to constrain Earth's redox state during the time between two rises of oxygen level. There are multiple pathways that impact the mobility of Cr in the environment. Since the redox pathway drew most of the attention from researchers, we conduct an ab initio study of the impact of redox-independent path on Cr isotope fractionation. Density functional theory (DFT) is employed in this study. Some complexes of Cr and organic ligands involved in redox-independent path are anionic molecules, which are expected to be suffered seriously by self-interaction error. The charge densities of these anionic molecules are delocalized in aqueous environment. However, there is no self-interaction error-free approximations available so far. Therefore, we introduced Fermi-Löwdin-orbital self-interaction corrected (FLOSIC) DFT to correctly describe the electronic structures of anionic molecules.

Investigation of Mineral Phase Effects Caused by Sulfer-Bearing Minerals in a Cumberland Simulant, using Laboratory Equipment

1P-42
3:30pm

Christine Knudson (699)

G. M. Perrett (Queen's University, Kingston, ON, Canada), A. C. McAdam (699), J. L. Campbell (University of Guelph, Guelph, ON, Canada), L. Sargent (University of Guelph, Guelph, ON, Canada), E. L. Flannigan (University of Guelph, Guelph, ON, Canada), R. V. Morris (NASA JSC), S. C. Andrejkovicova (699), S. A. Mertzman (Franklin and Marshall College, Lancaster, PA), S. W. Squyres (Cornell University, Ithaca, NY), P. R. Mahaffy (690)

The Mars Science Laboratory (MSL) rover payload is designed to assess the chemistry and mineralogy of surface materials encountered along its traverses through Gale Crater. The Alpha-Particle X-Ray Spectrometer (APXS) uses both Particle Induced X-Ray Emission (PIXE) and X-ray Fluorescence (XRF) to quantify elemental abundances. The Sample Analysis at Mars (SAM) suite of instruments constrains the mineralogy by detecting the volatiles evolved during sample pyrolysis (Evolved Gas Analysis (EGA)), and the Chemistry and Mineralogy (CheMin) instrument employs X-ray Diffraction (XRD) to identify and quantify crystalline minerals. These instruments can all constrain the amount of S in a sample; however, APXS indicates higher S concentrations in some samples than SAM. A mineralogical and chemical simulant of the Cumberland drill sample (CB) of the Sheepbed mudstone, analyzed at Gale Crater by MSL instruments between sols 282-408 was created to investigate the origin of these differences. Additional mixtures of the different CB minerals were created to investigate the influence of specific minerals on APXS- or SAM-derived S values. The mixtures range from simple two mineral mixtures to the full multi-phase simulant and were analyzed as pressed pellets by XRF and PIXE to approximate APXS analyses. EGA was also done on each of the mixtures under SAM-like conditions to quantify the amount of evolved SO2, and these results were compared to SAM EGA data from CB. These quantities were converted to equivalent SO_3 values and compared to the APXS-like measurements. Transmission XRD was done on the powders using a CheMin-like instrument, the CheMin-4. Preliminary results indicate that S quantities reported by SAM are underestimated because not all sulfur minerals completely evolve SO2 within the SAM temperature range. Additionally, the S quantities reported by APXS can be overestimated because of the mineral phase effects (MPEs), which arise due to the distribution of elements among different minerals. Additionally, preliminary CheMin-4 results suggest that particle density may be a factor affecting MSL CheMin crystalline mineral abundances.

1P-43
3:30pm

Effects of a Solar Flare on the Martian Hot O Corona and Photochemical Escape

Yuni Lee (699)

Chuanfei Dong, Dave Pawlowski, Valeriy Tenishev, Paul Mahaffy (690), Mehdi Benna (699), Michael Combi, Stephen Bougher, Frank Eparvier, Edward Thiemann

An X8.2-class solar flare occurred on September, 10th 2017, peaking at approximately 16:12 UT. In this study, we examined for the first time the flare-induced effects on the Martian hot O corona and resulting photochemical loss of O. We performed integrated one-way couplings of three numerical models, AMPS, M-GITM, and MF-MHD coupled with a custom spectral irradiance model. Our modeling study is designed to investigate the effects of the flare only and better capture the important atmospheric variability during the flare. We conducted simulations for four model cases, which are the time snapshots representing the flare phases. The rapid ionospheric response to the increase in the soft X-ray flux (∼800%) facilitates more hot O production at altitudes below the main ionospheric peak, but almost all of these atoms are thermalized before escape to space. In response to the simultaneous increase in the EUV flux (∼170%), the overall upper ionospheric and thermospheric densities are enhanced, and the peak thermospheric responses are found about 1.5 hours later. The photochemical escape rate increases by ∼20% with the abrupt increases in the soft X-ray and EUV fluxes but decreases rapidly by ∼13% about 2.5 hour later before recovering the pre-flare level. Since the escaping hot O atoms are mostly produced at high altitudes where ionization by the EUV flux is the greatest, the main contributor to the 20% increase in escape rate is the enhancement in the EUV flux.

1P-44
3:30pm

Salt Effects of Derivatization

Brian Leiter (699)

Jennifer Stern (699), Maeva Millan (699)

For a gas chromatographic mass spectrometer (GCMS) to properly detect amino acids, an amination reaction must first take place where the amino group is modified so that the product (derivative) will readily vaporize and interact with the GC column. Under ideal conditions, a specific reagent Dimethylformamide Dimethylacetal (DMFDMA) is known to react with amino acids and produce a detectable derivative. Water is known to react strongly with DMFDMA and produce derivatives of its own, however this competative reaction is heavily favored to the point where amino acid derivatives are not produced to a detectable level. For this reason, a sample must initially undergo a drying process before being subject to DMFDMA. Like with water, the presence of a salt compound may give similar competition though salts will simply not dry out of a sample and instead must be separated via adddditional process. Understanding the effects of salts on the derivatization reaction is essential for any subsequent processing. To evaluate the effects of salt on the derivatization process, mixtures of amino acids are subject to varying amounts and types of salts. If the present salts were to affect the amino acid derivatization process a trend would emerge correlating to the concentration of the present salt to the extent of the derivatization reaction. This

research began early July and is still underway. Initial results at low concentrations have shown that the type of salt present has a strong effect on the derivatization process.

Identifying Slow Solar Wind Sources

1P-45
3:30pm

Nathalia Alzate (670)
Nicholeen Viall (671)

The solar wind is a crucial physical link between the Sun and objects in the solar system. It contains signatures of the physical processes that heat the corona and accelerate the wind. Remote sensing and in situ data strongly suggest that much of the density variability observed in the slow solar wind is a tracer of solar wind formation. However, the nature of this connection has yet to be established. So far, identification of the source of the slow solar wind has been hampered by the complexity of plasma structures in the very low corona and data limitations in terms of noise reduction. We present our work in which we applied new state of the art image processing techniques to coronal imaging data from EUV and coronagraph instruments onboard the STEREO A and B spacecraft in an effort to push the limits of current instrumental sensitivity and resolution. We present results on the identification of the sources of the variable solar wind. Our work contributes to the broad effort to identify and characterize the types of coronal structures associated with the formation of the slow and variable solar wind.

Mapping the vertical distribution of water ice clouds on Mars with NOMAD/TGO

1P-46
3:30pm

Giuliano Liuzzi (693)
Geronimo Villanueva (693), Matteo Crismani (693), Michael J. Mumma (693)

We present profiles of water ice clouds retrieved from the data collected by the high-resolution Nadir and Occultation for MArs Discovery (NOMAD) instrument onboard the ExoMars / Trace Gas Orbiter (TGO). The NOMAD spectrometer is the first IR instrument capable of producing vertical profiles of aerosols with high spatial resolution of the order of 1 km. This is possible analyzing the data acquired in Solar Occultation geometry, which sample the atmosphere at different altitudes, hence permitting to quantify the extinction of the incoming direct solar radiation. Running a full retrieval of gases and aerosol opacity on the available Solar Occultation data, we have reconstructed several vertical profiles of ice clouds, and disentangled them from dust at each altitude. Looking at the spectral properties of ice extinction, we also provide a first characterization of the microphysical properties of ice crystals, and constrained the particle size and their vertical variation. This allows us to create a detailed 3-D map of ice clouds near the Martian terminator. Such a study opens a pathway to investigate in great detail the water condensation processes that occur in the Martian atmosphere, which can be more fully understood by the simultaneous retrieval of water ice, H2O and HDO profiles. This particular analysis is ongoing with NOMAD data. In addition, given the capability of NOMAD to map water ice clouds at very high vertical

sampling, a precise quantification of the vertical boundaries of clouds are a key aspect in improving the current understanding of their radiative effect and the induced heating rate. Following its successful orbital insertion in early 2018, we retrieved unique vertical profiles of several gas species and aerosols with ExoMars/TGO/NOMAD. In this paper, we report initial retrievals of water ice derived during this initial observational period (April-May 2018).

A Study of Martian Aerosols throughout the 2018 Planet Encircling Dust Event (PEDE) as observed by TGO/NOMAD and MAVEN/I

1P-47
3:30pm

Matteo Crismani (693)
Geronimo Villanueva (693), Giuliano Liuzzi (693)

The Nadir and Occultation for MArs Discovery (NOMAD) instrument suite onboard the ExoMars/Trace Gas Orbiter (TGO) observes in the ultraviolet and infrared wavelengths in both Solar Occultation and Nadir Mapping modes. TGO orbit tracks are 2 hours apart, which provides unprecedented mapping of dayside aerosols. We utilize this dataset to investigate the geographic distribution of ice and dust, before, during, and after the Planet Encircling Dust Event of 2018. Using IR channels that are typically transparent to the atmosphere but opaque to dust, we identify and complement vertical profiles of dust and ice taken in Solar Occultation geometry. We also compare these observations to the Imaging Ultraviolet Spectrograph (IUVS) onboard MAVEN, which was able to observe full disk images of aerosols and ozone during this time period.

Author Index